DR STEFANIE J. MUELLER-SCHUESSELE (Orcid ID : 0000-0003-4061-1175)

DR MARKUS SCHWARZLANDER (Orcid ID : 0000-0003-0796-8308)

Article type : Methods Paper

Methods

The fluorescent protein sensor roGFP2-Orp1 monitors *in vivo* H_2O_2 and thiol redox integration and elucidates intracellular H_2O_2 dynamics during elicitor-induced oxidative burst in Arabidopsis

Thomas Nietzel [a,b], Marlene Elsässer [a,b,c], Cristina Ruberti [a], Janina Steinbeck [a], José Manuel Ugalde [b], Philippe Fuchs [a,b], Stephan Wagner [a,b], Lara Ostermann [b,f], Anna Moseler [b], Philipp Lemke [a], Mark D. Fricker [d], Stefanie J. Müller-Schüssele [b], Bruno M. Moerschbacher [a], Alex Costa [e], Andreas J. Meyer [b,f], Markus Schwarzländer [a,b,*]

[a] Institute for Biology and Biotechnology of Plants, University of Münster, Schlossplatz 8, D-48143 Muenster, Germany

[b] Institute of Crop Science and Resource Conservation (INRES), University of Bonn, Friedrich-Ebert-Allee 144, D-53113 Bonn, Germany

[c] Institute for Cellular and Molecular Botany (IZMB), University of Bonn, Kirschallee 1, D-53115 Bonn, Germany

[d] Department of Plant Sciences, University of Oxford, South Parks Road, Oxford, OX1 3RB, UK

[e] Dipartimento di Bioscienze, Università degli Studi di Milano, I-20133 Milano, Italy

[f] BioSC, c/o Forschungszentrum Jülich, D-52425 Jülich, Germany

This article has been accepted for publication and undergone full peer review but has not been through the copyediting, typesetting, pagination and proofreading process, which may lead to differences between this version and the Version of Record. Please cite this article as doi: 10.1111/nph.15550

* *Correspondence*
Markus Schwarzländer, Schlossplatz 8, 48143 Münster, Germany
phone number: +49 251 83 24801
e-mail: markus.schwarzlander@uni-muenster.de

Received: *8 September 2018*
Accepted: *13 October 2018*

ORCIDs: Thomas Nietzel, http://orcid.org/0000-0002-1934-1732; Cristina Ruberti, https://orcid.org/0000-0002-9013-1412; Janina Steinbeck, http://orcid.org/000-0002-7793-5053;
José Manuel Ugalde, https://orcid.org/0000-0002-0601-4302; Philippe Fuchs, http://orcid.org/0000-0001-6379-853X; Stephan Wagner, http://orcid.org/0000-0001-5369-7911; Mark D Fricker, http://orcid.org/0000-0002-8942-6897; Stefanie J Müller-Schüssele, https://orcid.org/0000-0003-4061-1175; Bruno M Moerschbacher, https://orcid.org/0000-0001-6067-3205; Alex Costa, http://orcid.org/0000-0002-2628-1176; Andreas J Meyer, http://orcid.org/0000-0001-8144-4364; Markus Schwarzländer, http://orcid.org/0000-0003-0796-8308

Summary

- Hydrogen peroxide (H_2O_2) is ubiquitous in cells and at the centre of developmental programmes and environmental responses. Its chemistry in cells makes H_2O_2 notoriously hard to detect dynamically, specifically and at high resolution. Genetically encoded sensors overcome persistent shortcomings, but pH sensitivity, silencing of expression and a limited concept of sensor behaviour *in vivo* have hampered meaningful H_2O_2 sensing in living plants.
- We establish H_2O_2 monitoring in the cytosol and the mitochondria of Arabidopsis with the fusion protein roGFP2-Orp1 using confocal microscopy and multiwell fluorimetry.
- We confirm sensor oxidation by H_2O_2, show insensitivity to physiological pH changes, and demonstrate that glutathione dominates sensor reduction *in vivo*. We show the responsiveness of the sensor to exogenous H_2O_2, pharmacologically-induced H_2O_2 release, and genetic interference with the antioxidant machinery in living Arabidopsis tissues. Monitoring intracellular H_2O_2 dynamics in response to elicitor exposure reveals late and prolonged impact of the oxidative burst in the cytosol, which is modified in redox mutants.
- We provide a well-defined toolkit for H_2O_2 monitoring *in planta* and show that intracellular H_2O_2 measurements only carry meaning in the context of the endogenous thiol redox systems. This opens new possibilities to dissect plant H_2O_2

dynamics and redox regulation, including intracellular NADPH-oxidase-mediated ROS signalling.

Keywords: H_2O_2, glutathione, mitochondria, cytosol, fluorescent protein sensors, *in vivo* imaging, flg22, NADPH oxidase

Introduction

Hydrogen peroxide (H_2O_2) occurs ubiquitously in aerobic cells and organisms. An ever-growing body of evidence has associated H_2O_2 with central physiological, pathological and signalling processes (Smirnoff & Arnaud, 2018; Waszczak *et al.*, 2018). The importance of well-controlled H_2O_2 dynamics in plants is reflected by a comprehensive inventory of both H_2O_2-generating systems and antioxidant proteins. Production of H_2O_2, or superoxide as its precursor, occurs in all cell types and in most subcellular compartments, at rates that are strongly dependent on metabolic activity and environmental conditions. Although it is notoriously difficult to quantify the relative contribution of different mechanisms to total H_2O_2 production *in vivo*, specific steps in the photosynthetic and respiratory electron transport chains, peroxisomal carbon metabolism and cell wall peroxidases as well as plasma membrane NADPH oxidases are often assumed to dominate cellular H_2O_2 production. Yet, other redox active proteins, such as the flavoenzymes involved in central metabolism and oxidative protein folding, are also able to reduce molecular oxygen to H_2O_2, and may turn into sources of major H_2O_2 flux under specific conditions (Meyer *et al.*, 2018).

H_2O_2 and other reactive oxygen species (ROS) were regarded toxic by-products of an aerobic lifestyle for decades. It is now under debate whether H_2O_2 generation by metabolism and the electron transport chains is really an unavoidable side effect. Alternatively, it may be evolutionary optimised to serve specific signalling and only turn pathological under extreme conditions when imbalance arises between the rates of ROS production and scavenging. More evidently, NADPH oxidases operate as professional ROS-generating systems that act both as cellular signalling hubs and integrators of long distance signalling. Their contribution to a range of signalling and developmental systems such as regulation of stomatal aperture (Pei *et al.*, 2000; Kwak *et al.*, 2003; Sierla *et al.*, 2016; Devireddy *et al.*, 2018), root hair development (Foreman *et al.*, 2003), pollen tube growth (Potocky *et al.*, 2007; Boisson-Dernier *et al.*, 2013; Lassig *et al.*, 2014), Casparian strip formation (Lee *et al.*, 2013), organ separation (Lee *et al.*, 2018) and biotic stress responses (Chaouch *et al.*, 2012; Kadota *et al.*, 2014; Siddique *et al.*, 2014) is well established. Furthermore, in current models of long distance signalling, H_2O_2 derived from NADPH oxidase has been proposed as a major second messenger in cell-to-cell signalling, that

works in tight mechanistic association with intracellular Ca^{2+} dynamics (Miller *et al.*, 2009). Concepts established for Ca^{2+} signalling, such as signatures and micro-domains, have also been discussed for ROS signalling (Choudhury *et al.*, 2017), but experimental evidence is lacking due to the lack of comparable tools to monitor intracellular ROS dynamics in living cells and tissues. Even attractive signalling concepts, such as ROS waves running through tissues to relay systemic signals, are based on indirect transcriptional evidence, such as luciferase fused to the promoters of *GST1* and *ZAT12* (Grant *et al.*, 2000; Miller *et al.*, 2009), from which the precise spatiotemporal ROS dynamics can only be inferred, and the specific cellular targets remain unknown. The large body of indirect data for intracellular ROS signalling, such as genetic or transcriptional evidence, reflects the complex situation that arises from the reactive and chemically diverse nature of ROS. In combination with the technical shortcomings in the available tools, a double challenge arises for progress towards a detailed understanding of ROS signalling.

Similar problems arise with decoding H_2O_2 signals. Thiol oxidation by H_2O_2 has been identified as the mechanism of H_2O_2 sensing in several pathways in bacteria, yeast and animal systems (Zheng *et al.*, 1998; Delaunay *et al.*, 2002; Peralta *et al.*, 2015; Sobotta *et al.*, 2015). H_2O_2 can directly oxidise protein thiols, but such a mechanism is unlikely to occur indiscriminately *in vivo*, where oxidation is typically mediated by a small number of highly reactive thiols located on a specific subset of proteins (Veal *et al.*, 2007; Weerapana *et al.*, 2010). Specific cysteine thiols, such as the catalytic thiols of the peroxiredoxins, are orders of magnitude more reactive towards H_2O_2 than most other cellular thiols, making them by far the preferred target of oxidation in the presence of physiological H_2O_2 fluxes. Subsequently, the initial oxidation of these reactive thiols can be transmitted to other proteins by redox relays. A well-studied example is the yeast oxidant receptor peroxidase-1/ glutathione peroxidase 3 (Orp1/Gpx3), which shows a particularly high reactivity with H_2O_2 and mediates the targeted oxidation of the YAP1 transcription factor (Delaunay *et al.*, 2002). By analogy to Ca^{2+}-binding proteins, these peroxidases provide a mechanism for signal specificity, based on constrained protein-protein interactions and reactivity, to trigger a defined response.

To understand which specific regulatory processes involve H_2O_2 signalling, at which precise subcellular location, and at which developmental stage, the specific and direct detection of H_2O_2 *in planta* would be a major advance. While *in vitro* or extracellular detection of H_2O_2 is well established (Gomes *et al.*, 2005; Ortega-Villasante *et al.*, 2018; Rezende *et al.*, 2018), intracellular measurements *in vivo* of H_2O_2 still suffer from major technical constraints (Marchesi *et al.*, 1999; Buettner, 2015). The initial introduction of genetically encoded Ca^{2+} sensors brought transformative insights into plant Ca^{2+} dynamics and signalling. The introduction of redox-sensitive GFP sensors has started a comparable process for redox regulation (Schwarzländer *et al.*, 2016). Nevertheless, *in vivo*

measurements of intracellular H_2O_2 dynamics comparable to those of free Ca^{2+} have remained problematic. RoGFP sensors specifically monitor dynamics of the glutathione redox potential (E_{GSH}) with subcellular resolution. The variant roGFP2 fused to human glutaredoxin 1 (Grx1-roGFP2) shows very low reactivity with H_2O_2 in comparison to competing endogenous thiols of specialised H_2O_2 detoxifying enzymes (Schwarzländer *et al.*, 2016), but is specific for E_{GSH} (Gutscher *et al.*, 2008). Several other sensor variants have been engineered to enable specific *in vivo* monitoring of H_2O_2. A common approach is to fuse an H_2O_2-reactive domain, from a peroxidase for example, to give H_2O_2 specificity, to a fluorescent protein allowing dynamic detection via changes in its optical properties. Sensors of the HyPer family (Belousov *et al.*, 2006; Markvicheva *et al.*, 2011; Bilan *et al.*, 2013; Ermakova *et al.*, 2014), and the roGFP-based proximity sensors, roGFP2-Orp1 and roGFP2-Tsa2 (Gutscher *et al.*, 2009; Morgan *et al.*, 2016) have emerged as two dominant H_2O_2 biosensor classes. More recently, a novel FRET sensor based on human peroxiredoxin 2 has been introduced (Langford *et al.*, 2018).

HyPer-based measurement of H_2O_2 has been performed in Arabidopsis (Costa *et al.*, 2010; Hernandez-Barrera *et al.*, 2013; Hernandez-Barrera *et al.*, 2015; Rodrigues *et al.*, 2017), as well as in transiently transformed tobacco leaves (Exposito-Rodriguez *et al.*, 2017). However, the circular permutated yellow fluorescent protein (cpYFP) chromophore used in HyPer is highly pH-sensitive (Ezerina *et al.*, 2014; Schwarzländer *et al.*, 2014), complicating any unambiguous data interpretation without simultaneous measurement and correlation for local pH. Indeed, several studies have shown that a HyPer response was caused by pH changes and not, or only partially, by H_2O_2 (Roma *et al.*, 2012; Weller *et al.*, 2014). A redox insensitive Cys-mutant of HyPer, named SypHer, was subsequently introduced (Poburko *et al.*, 2011), which is strictly required as a pH control in HyPer experiments. Despite this elegant workaround, each HyPer variant requires a matching SypHer variant (Matlashov *et al.*, 2015), increasing measurement complexity and data analysis, and even SypHer cannot precisely mimic the exact pH characteristics of HyPer in its different redox states. Differences in the exact pH responses between dyes and sensors (*e.g.*, different pK_a or dynamic range) is a general problem for pH controls and serious misinterpretations have arisen from this issue (Schwarzländer *et al.*, 2012b). In contrast, the roGFP2-based sensors used to monitor E_{GSH} are pH-insensitive over a physiological pH range (Schwarzländer *et al.*, 2008; Albrecht *et al.*, 2011) and provide an alternative chromophore for sensor construction.

In the fusion sensor roGFP2-Orp1, reaction of Orp1 with H_2O_2 results in the formation of a sulfenic acid (-SOH) with its reactive cysteine Cys^{36} (Delaunay *et al.*, 2002), which then condenses with Cys^{82} to generate an intramolecular disulfide (Gutscher *et al.*, 2009; Albrecht *et al.*, 2011) **(Fig. 1a)**. The disulfide bridge is transferred to the reduced roGFP2 by thiol-

disulfide exchange due to the high local concentration arising from the close proximity, which changes the steric arrangement of the beta barrel surface and in turn the optical characteristics of the chromophore. Probe oxidation is reversed by reduction, and the cellular thiol redox machinery appears to deliver the required electrons *in vivo*, which is the basis for any dynamic monitoring of H_2O_2 changes. The contribution of the individual cellular redox pathways to the *in vivo* reduction of the probe has remained undefined. Likewise, for the HyPer sensors, experimental data on the pathway for the re-reduction of the sensor is missing. Since it is the balance between the oxidation and reduction kinetics of the probe that sets its redox state and spectroscopic read-out, knowledge about the interacting reducing system is essential for meaningful interpretation of any dynamic H_2O_2 sensor response (discussed at detail in Schwarzländer *et al.*, 2016). Free roGFP2 protein equilibrates with E_{GSH} (Meyer *et al.*, 2007; Schwarzländer *et al.*, 2008), whereas the reduction of free Orp1 was found to be mediated by the thioredoxin machinery (Delaunay *et al.*, 2002). RoGFP2-Orp1 was exploited to monitor H_2O_2 dynamics in yeast (Bode *et al.*, 2013), Drosophila (Albrecht *et al.*, 2011) and human cells (Gutscher *et al.*, 2009; Sobotta *et al.*, 2013). Very recently the cytosolic construct was introduced into *Cyclamen persicum* (Ratjens *et al.*, 2018), and we have previously used it in Arabidopsis guard cells (Scuffi *et al.*, 2018). Nevertheless, detailed characterisation of the sensor in plants and its application in different cell compartments has been lacking.

Here, we validate roGFP2-Orp1 to monitor subcellular H_2O_2 dynamics in Arabidopsis *in vivo*. First, we establish Arabidopsis sensor lines with cytosolic and mitochondrial sensor expression. Second, we characterise the sensor *in vitro* by reconstitution of its potential interacting redox systems. Third, we examine its behaviour *in vivo* using chemical, pharmacological and genetic modulation of H_2O_2 exposure and thiol redox balance by confocal microscopy at high resolution or multiwell fluorimetry for high throughput. Forth, we demonstrate that the sensor system is sufficiently sensitive to allow direct analysis of intra- and subcellular H_2O_2 and redox signalling, as exemplified by elicitor-induced NADPH-oxidase activation.

Materials & Methods

The following procedures are described in **Supporting Information Methods S1-S4**: Cloning of sensor constructs and generation of plant lines; Plant culture; Purification of recombinant proteins; Elicitors. Primers used in this work are given in **Supporting Information Table S1**.

In vitro characterisation of roGFP2-Orp1

The fluorescence characteristics of purified roGFP2-Orp1 (5 µM) were analysed in a spectro-fluorometer (JASCO FP-8300, Tokyo, Japan). Excitation spectra of roGFP2-Orp1 in the range of 360 - 510 nm (with 1 nm resolution and 5 nm bandwidth) were recorded with emission in the range of 512.5 – 517.5 nm in potassium phosphate buffer (100 mM, pH 7.0) supplemented with 5 mM EDTA. Emission spectra of oxidised and reduced roGFP2-Orp1 in the range of 500 - 600 nm were recorded with 1 nm resolution and 5 nm bandwidth at excitation at either 405 nm or 488 nm. Purified sensor was either reduced by 20 mM dithiothreitol (DTT) or oxidised by 1 mM 2,2-dithiopyridylsulfide (DPS).

Multiwell plate reader-based fluorimetry

RoGFP2-Orp1 was excited sequentially at 400 ± 5 nm and 482 ± 8 nm in a CLARIOstar plate reader (BMG Labtech, Ortenberg, Germany) and emission was recorded at 520 ± 5 nm. For excitation scans, roGFP2-Orp1 was exited in 1 nm steps with 10 nm bandwidth; emission was recorded in the range of 515-525 nm. The internal temperature was kept constant at 25°C. 7-day-old seedlings or leaf discs of 4 week-old plants were filled in transparent 96-well plates, except for the luminol assay, where white 96-well plates were used (Sarstedt, Nümbrecht, Germany). Fluorescence of Col-0 plants was recorded and subtracted from all data before analysis. For *in vivo* experiments with Arabidopsis seedlings and leaf discs, plant material was submerged in 10 mM MES, pH 5.8, 5 mM KCl, 10 mM $MgCl_2$, 10 mM $CaCl_2$. For the leaf disc assays, plates were kept in the dark overnight and buffer was exchanged before starting the assay. For *in vitro* assays, purified roGFP2-Orp1 was analysed in potassium phosphate buffer (100 mM, pH 7.0) supplemented with 5 mM EDTA, if not elsewhere specified.

Confocal imaging and image analysis

Confocal imaging of 5-day-old Arabidopsis seedlings was performed at 20℃ using either a Leica DMI 6000B inverted microscope equipped with a Leica TCS SP5 laser scanning device for generating the seedling map or a Zeiss LSM780 microscope as described previously (Wagner *et al.*, 2015). RoGFP2-Orp1 was excited sequentially at 405 nm and 488 nm and emission was recorded at 505 to 535 nm, with the pinhole set to 5 airy units. Auto fluorescence was collected at 425 to 475 nm and chlorophyll fluorescence at 670 to 720 nm. MitoTracker Orange CMTMRos was excited at 543 nm and emission was recorded at 570-620 nm. Single plane images were processed with a custom MATLAB-based software (Fricker, 2016) using x,y noise filtering and fluorescence background subtraction.

Results

Generation of Arabidopsis lines for the expression of roGFP2-Orp1 in the cytosol and the mitochondrial matrix

We generated Arabidopsis lines expressing the fusion construct roGFP2-Orp1 in the cytosol and the mitochondrial matrix. Twelve independent lines with different expression levels for both subcellular compartments were initially selected based on fluorescence intensity and two lines each were propagated to homozygosity. Although severe silencing has been a reoccurring problem in plant *in vivo* sensing (Pei *et al.*, 2000; Deuschle *et al.*, 2006; Chaudhuri *et al.*, 2008; Jones *et al.*, 2014; Behera *et al.*, 2015; Loro *et al.*, 2016; Schwarzländer *et al.*, 2016), we found the constitutive expression to be stable across generations.

The fluorescence in cotyledon epidermal cells of the cyt-roGFP2-Orp1 lines showed characteristic fluorescence in the cytosol and the nucleus **(Fig. 1b)**. The signal was restricted to a thin layer between plasma membrane and vacuole, to trans-vacuolar strands, and to the nucleoplasm counterstaining the nucleolus. The mt-roGFP2-Orp1 lines showed characteristic fluorescence distribution for plant mitochondria (El Zawily *et al.*, 2014), and co-localised with the mitochondrial matrix marker MitoTracker® Orange CMTMRos **(Fig. 1c)**. We observed consistently unambiguous cytosolic or mitochondrial sensor localisation independent of tissue type and developmental stage.

The cyt-roGFP2-Orp1 plants showed a wild type phenotype, while the mt-roGFP2-Orp1 lines were delayed in their growth **(Fig. 1d)** reminiscent of other lines expressing fluorescent biosensors in the mitochondrial matrix, irrespective of sensor type (De Col *et al.*, 2017). The combination of both the cytosolic and the mitochondrial lines provided us with a setup to explore live monitoring of H_2O_2 with subcellular resolution. For further *in planta* analyses lines #1 were used.

Sensor protein is insensitive to pH and gives an integrated response to H_2O_2 and the thiol redox systems in vitro

To draw reliable interpretations from *in planta* measurements we initially characterised the sensor protein properties *in vitro*. The responsiveness of the roGFP2-Orp1 fusion sensor to H_2O_2 and its specificity have been demonstrated previously (Gutscher *et al.*, 2009). To fill remaining gaps in our understanding of the pH sensitivity and reversible sensor behaviour, we characterised the behaviour of roGFP2-Orp1 protein *in vitro*. Excitation and emission scans confirmed the typical dual excitation and single emission properties of roGFP2-based probes (Dooley *et al.*, 2004; Hanson *et al.*, 2004) from the fluorescent reporter domain of the fusion protein (Gutscher *et al.*, 2009) **(Fig. 2a)**. RoGFP2-Orp1, reduced by 20 mM dithiothreitol (DTT), showed a characteristic peak at around 490 nm

excitation, while the sensor that was oxidised by 1 mM 2,2-dithiopyridylsulfide (DPS) showed two peaks at about 400 nm and 490 nm. The shift between the two excitation maxima was ratiometric with a spectroscopic dynamic range (δ) of 6.1, as calculated for excitation at 405 and 488 nm (laser wavelengths typically available for confocal microscopy). Emission spectra of both roGFP2-Orp1$_{red}$ and roGFP2-Orp1$_{ox}$ showed a common maximum at around 515 nm **(Supporting Information Fig. S1b,c)**.

Excitation ratios of purified roGFP2-Orp1 were constant in the pH range from 6.5 to 8.3 for both the oxidised and the reduced state, resulting in a stable spectroscopic dynamic range **(Fig. 2b)**. Decreasing pH below 6 led to a gradual decrease in the dynamic range. pH stability within the physiological range provides a critical advantage in both the plant cytosol and the mitochondrial matrix, where pH can fluctuate considerably (*e.g.*, Felle, 2001; Schwarzländer *et al.*, 2012a; Behera *et al.*, 2018).

Next we assayed the sensor response to H_2O_2 **(Fig. 2c,d)**. Pre-reduced roGFP2-Orp1 was titrated with H_2O_2 concentrations that covered the range around the reaction stoichiometry of the sensor (0.3 µM of sensor protein as quantified by Bradford assay). Untreated, reduced roGFP2-Orp1 showed a steady rate of spontaneous oxidation, reflecting the high sensitivity of the sensor to oxidation even in the de-gassed media. H_2O_2 caused a dose-dependent increase in sensor oxidation. One µM of H_2O_2 was sufficient to oxidise the roGFP2-Orp1 population completely, while sub-stochiometric amounts caused clear, but more modest oxidation **(Fig. 2d)**. Considering that oxidation of one sensor molecule can involve between one and two H_2O_2 molecules (one each for the Orp1 and the roGFP2 disulfides), the responses of the sensor match the predicted reaction stoichiometry range. The addition of 0.25 µM H_2O_2 resulted in an oxidation rate that was close to half of the maximal rate reached around 1 µM **(Fig. 2d; Supporting Information Fig. S1d)**. Addition of DTT efficiently reduced the sensor, confirming the reversibility of the response in the presence of appropriate reductant.

The steady state of the sensor is set by the relative rates of oxidation and reduction. We reconstituted both the thioredoxin and the glutathione systems *in vitro* to estimate the respective contribution of both major cellular thiol redox pathways to the reduction of the sensor **(Fig. 2c,e)**. The roGFP2-Orp1 population was oxidised after purification and could not be further oxidised by DPS. Reconstitution of the thioredoxin machinery by addition of NADPH, NADPH-dependent thioredoxin reductase b (NTRb; localised in the Arabidopsis cytosol and the mitochondrial matrix; Reichheld *et al.*, 2007); and TRX-O1 (the dominating Arabidopsis thioredoxin in the mitochondrial matrix; Laloi *et al.*, 2001; Gelhaye *et al.*, 2004); caused steady reduction of the sensor extract. Likewise, addition of glutathione (GSH), in the presence of non-limiting amounts of NADPH and yeast glutathione reductase (GR), led to reduction by a gradual ratio decrease towards a partially reduced steady state. In the

presence of Arabidopsis glutaredoxin C1 (GRXC1), addition of glutathione caused a much faster reduction and reached a plateau at a largely reduced state. The data indicate that both cellular redox machineries are capable of reducing the roGFP2-Orp1, but the glutathione/GRX system was kinetically more effective than the thioredoxin system.

The in vivo responses to H_2O_2 demonstrate sensor functionality in planta

To test whether the *in vitro* characteristics of the sensor protein are valid *in vivo*, we first assessed the redox state of the roGFP2-Orp1 sensor in the cytosol across an entire Arabidopsis seedling by confocal microscopy (**Fig. 3a; Supporting Information Fig. S2**). The 405/488 nm excitation ratio was remarkably stable across the plant, and deviations that were occasionally observed in individual seedlings did not turn out to be systematic. Such homogeneity was different to recent findings with roGFP2-Orp1 in Drosophila embryos (Albrecht *et al.*, 2011) and with biosensors of other specificities in Arabidopsis (De Col *et al.*, 2017).

To test the *in vivo* responsiveness of cytosolic roGFP2-Orp1 to external DTT and H_2O_2 we focussed on the root tip **(Fig. 3b,c)**. Excessive concentrations were used to guarantee sensor saturation. H_2O_2 caused an increase in excitation ratio whilst DTT caused no change in the cytosolic signal. By contrast, the mitochondrial roGFP2-Orp1 was further reduced from resting levels by DTT, indicating slight oxidation of the sensor at steady state. The spectroscopic dynamic range (δ) was 6.5 for the cytosolic roGFP2-Orp1 and 4.1 for the mitochondrial roGFP2-Orp1. These data show that roGFP2-Orp1 responds dynamically to H_2O_2 *in planta*.

In conjunction with confocal imaging, we adapted multiwell fluorimetry (De Col *et al.*, 2017) to monitor H_2O_2 dynamics *in planta* with increased throughput and over time. Ratiometric measurements make the sensor readings independent of expression level, as well as tissue amount in the well, as long as the sensor signal is sufficiently high compared to the background. Redox responses of intact Arabidopsis seedlings as determined by multiwell fluorimetry resulted in dynamic range values that were comparable to those measured in root tips by confocal microscopy **(Fig. 3; Supporting Information Fig. 3a)** and were not significantly different between independent sensor lines. To assess the validity of those measurements we recorded excitation spectra from seedlings expressing cyt-roGFP2-Orp1 and mt-roGFP2-Orp1 **(Fig. 4a,b; Supporting Information Fig. 3b)**. The tissues displayed raw fluorescence spectra similar to the characteristic shape observed *in vitro* **(Fig. 2a)** and the relative fluorescence in the non-sensor-expressing controls was low, indicating that chlorophyll fluorescence did not cause a significant interference. However, increasing auto-fluorescence intensities with excitation in the UV region were observed, and this background made a significant impact on the overall spectrum for the dimmer mitochondrial

lines. Nevertheless, the sensor signal was distinguishable from background fluorescence at excitation around 400 nm even in the reduced sensor **(Supporting Information Fig. 3b)** and subtraction of the control fluorescence resulted in spectra that were equivalent to those of the purified sensor protein **(Fig. 2a)**, demonstrating that quantitative measurements can be performed unperturbed by tissue auto-fluorescence. The corresponding 2D spectra confirmed that sensor fluorescence was high as compared to the background across the relevant excitation space **(Supporting Information Fig. S4)**.

To investigate if, and how quickly, endogenously produced H_2O_2 can oxidise roGFP2-Orp1 *in vivo*, we made use of the setup for dynamic monitoring after menadione application to Arabidopsis seedlings. Menadione mediates superoxide formation through the catalytic transfer of electrons from endogenous donors, such as the ubiquinone pool of the mitochondrial electron transport chain, to molecular oxygen. Superoxide in turn rapidly dismutates to H_2O_2. The effectiveness of the treatment with menadione at a sub lethal level (30 µM; Lehmann *et al.*, 2009) was validated with the broadly used, but unspecific and irreversible ROS probe H_2DCF-DA **(Supporting Information Fig. S5a)**. DCF fluorescence increased instantly in response to the treatment at a higher rate than in the solvent control. A similarly rapid oxidation response was observed with cytosolic roGFP2-Orp1, which could be observed as a progressive ratiometric shift in the *in vivo* spectrum **(Fig. 4c,d)**. Menadione triggered oxidation in both the cytosol and the mitochondrial matrix, albeit with different kinetics, and across the different tissue types observed by confocal microscopy (**Supporting Information Fig. S5b,c**). This demonstrates the sensor is responsive *in planta* and shows that both confocal imaging and multiwell fluorimetry allow *in vivo* monitoring of H_2O_2 with subcellular specificity.

Genetic impairment of subcellular redox machineries identifies the glutathione system as the dominating mechanism of sensor reduction in planta

Since the dynamic response characteristics of the sensor are shaped by the relative rates of oxidation and reduction, we aimed to explore the impact of varying the reducing and antioxidant systems *in vivo*. We introduced the cytosolic and mitochondrial roGFP2-Orp1 sensor into a set of different Arabidopsis mutant backgrounds with impairment of their subcellular redox machineries.

Established lines with disruption of cytosolic or mitochondrial glutathione- and thioredoxin-based redox machineries were selected to interfere with the potential reduction pathways of roGFP2-Orp1; *ntra/b* (Reichheld *et al.*, 2007)*, trx-o1* (Daloso *et al.*, 2015), *gr1* (Marty *et al.*, 2009) and *gr2* (L. Marty *et al.*, unpublished) **(Fig. 5a)**. We anticipate that these mutants may have altered steady state H_2O_2 levels, because the missing pathways normally supply electrons for H_2O_2 detoxification by peroxidases. In addition, *cat2-1*, impaired in

catalase 2 (Queval *et al.*, 2007; Kerchev *et al.*, 2016), as a high capacity sink for H_2O_2 in the peroxisomes, *sapx* impaired in ascorbate peroxidase activity in the plastid stroma and the mitochondrial matrix (Giacomelli *et al.*, 2007), as well as *prxII F*, impaired in mitochondrial matrix peroxiredoxin-II F (Finkemeier *et al.*, 2005) were selected **(Fig. 5a)**.

The cytosolic sensor indicated no change for most of the mutant backgrounds at steady state in any of the four investigated seedling areas **(Fig. 5b)**. The exception was *gr1* where a pronounced oxidative shift was observed in all the seedling areas. The mitochondrial sensor showed analogous oxidation in the *gr2* background, but interestingly increased oxidation was also detectable across the *gr1* seedlings. Oxidation was also found in the roots and root tips in the *cat2-1* and the *sapx* backgrounds, but not in the hypocotyl and the cotyledons. The *ntra/b*, *trx-o1* and *prx IIF* backgrounds showed no change in the mitochondrial matrix in any of the tissues.

Impairment of glutathione reductase in the cytosol (GR1) and the mitochondrial matrix (GR2) explains the strong oxidation of the cytosolic and mitochondrial sensor in those backgrounds, and provides *in vivo* evidence for a dominant role of the glutathione redox machinery in sensor reduction. By contrast, impairment of the thioredoxin machinery in the *ntra/b* and *trx-o1* backgrounds did not have any detectable impact on sensor oxidation. The minor oxidation of the mitochondrial sensor in the *gr1* background where cytosolic, but not mitochondrial, glutathione reductase activity is impaired, may suggest oxidation of the sensor due to a lack of antioxidant capacity in the cytosol, possibly by H_2O_2 diffusion from the cytosol into the matrix. A potential problem due to partial sensor mis-localisation in the cytosol appears unlikely based on microscopic inspection *gr1* sensor seedlings. Since catalase 2 is localised in the peroxisome, the effect in the mitochondria of root tissues may also be explained by H_2O_2 diffusion across the organelle membranes. An oxidative shift in the absence of sAPX suggests a role in mitochondrial H_2O_2 handling that cannot be compensated for efficiently in the roots.

To assess how steady state oxidation of the sensor affects the sensor dynamics in response to H_2O_2, we focussed on the cytosolic sensor in the wild type and the *gr1* background using multiwell fluorimetry **(Fig. 5c)**. While external application of H_2O_2 led to minor sensor oxidation followed by recovery towards the baseline, the response was stronger in the *gr1* background and recovery was delayed, demonstrating that decrease of antioxidant capacity and of the capacity for sensor re-reduction provides a genetic means to magnify the sensitivity to *in vivo* H_2O_2 transients.

Monitoring intracellular H_2O_2 dynamics during the elicitor-induced oxidative burst captures subcellular ROS signalling

The contrasts between compartments revealed in the different mutant backgrounds allowed us to address the question of how NADPH oxidase (RBOH)-derived apoplastic H_2O_2 would impact on intracellular H_2O_2 dynamics. Passage of extracellular H_2O_2 across the plasma membrane via aquaporins has been shown by several studies (Bienert & Chaumont, 2014; Rodrigues *et al.*, 2017; Bestetti *et al.*, 2018), but detailed assessment of subcellular impacts *in vivo* is lacking. To explore the intracellular impact of RBOH activation, we used multiwell fluorimetry and three different elicitor treatments; the N-terminal flagellin fragment flg22, a partially acetylated chitosan (DA 50%) and a fully deacetylated chitosan (DA 0%) (Melcher & Moerschbacher, 2016; Gubaeva *et al.*, 2018) **(Fig. 6a)**. While both chitosan treatments of leaf tissue expressing cytosolic roGFP2-Orp1 did not differ from the control, flg22 induced extended transient oxidation starting after about one hour of treatment and peaking at about two hours. The flg22 response was fully abolished by diphenyleneiodonium (DPI) confirming that the oxidation was due to induction of RBOH **(Fig. 6a inset;** note that DPI alone leads to gradual sensor oxidation probably due to inhibition of other flavoenzymes such as glutathione reductase; **Supporting Information Fig. S6)**. The sensor recordings showed excellent reproducibility of the qualitative response, while the amplitude was more variable between the individual biological replicates. Control measurements using extracellular luminol showed a much earlier transient, peaking at about 4 min, suggesting different dynamics between the extracellular and the intracellular responses **(Fig. 6b)**. Furthermore, an extracellular transient was also detected for the partially acetylated chitosan (DA 50%), peaking at about 10 min, while the response to the fully deacetylated chitosan (DA 0%) was very low and delayed to over 20 min. To address a potential sensitivity limitation of the assay by efficient cytosolic H_2O_2 scavenging and/or the effective sensor reduction, we performed the experiments in the *gr1* background (Marty *et al.*, 2009) **(Fig. 6c)**. As observed in **Fig. 5b and c**, the steady state of cytosolic roGFP2-Orp1 in the *gr1* background was strongly shifted towards oxidation in this background. Oxidation started early and showed an increased amplitude in response to flg22 as compared to the wild type background. Also partially acetylated chitosan (DA 50%) showed a clear cytosolic response, while the fully deacetylated chitosan (DA 0%) did not induce a detectable response. The peak amplitudes showed a clear increase in *gr1* as compared to WT **(Fig. 6c,d)** and correlated with the luminol controls **(Fig. 6b)**. The intracellular transient detected by roGFP2-Orp1 was nevertheless strongly extended, exceeding the four hours duration of the measurement. One mechanism to account for the difference in timing may be a secondary release of H_2O_2 from intracellular sources, like the mitochondrial electron transport chain, as suggested for mammalian systems (Dikalov, 2011). However, the mitochondrial-targeted

roGFP2-Orp1 sensor did not show any oxidation in response to flg22 in the wild type background, and even in the *gr2* background only a minor and early transient was detectable **(Fig. 6e)**. This suggests that H_2O_2 can reach the mitochondrial matrix, but that an active contribution by the mitochondria to cytosolic oxidation is unlikely. NADPH oxidase-derived H_2O_2 entered the cytosol at a sufficient rate to be sensed, despite efficient scavenging and sensor reduction by the antioxidant systems **(Fig. 6f)**. Technically, the usage of the *gr1* and *gr2* backgrounds offers an elegant means to increase detection sensitivity and to explore the contributions from different cell compartments to H_2O_2 release and signalling.

Discussion

Monitoring intracellular H_2O_2 dynamics in plants has been a long-standing challenge. Establishing roGFP2-Orp1 as a sensor for subcellular H_2O_2 monitoring *in planta* provides a toolkit, along with the critical conceptual framework, to experimentally unlock plant cell H_2O_2 dynamics and signalling. The straightforward expression of the sensor in Arabidopsis is in contrast to HyPer2 and roGFP2-Grx1 for which severe silencing and subcellular mis-targeting were reported (Exposito-Rodriguez *et al.*, 2013; Albrecht *et al.*, 2014; Exposito-Rodriguez *et al.*, 2017). Nevertheless, the mitochondrial sensor lines showed developmental delay, similar to other mitochondrial sensor lines (De Col *et al.*, 2017), which requires critical consideration in the interpretation of measurements. We further provide a mechanistic framework for the operation of the sensor *in vivo*, based on *in vitro* reconstitution analyses and characterisation in several genetic mutant lines impaired in H_2O_2 handling and thiol redox regulation. Experimental validation of such a concept has not been available for any H_2O_2 sensor in plants, but is critical for meaningful interpretation of *in vivo* measurements (Schwarzländer *et al.*, 2016). Our data extend the H_2O_2 sensing concept to an electron flux model in which an irreversible reaction between H_2O_2 and the probe is balanced by reduction/redox equilibration with glutathione as mediated by glutaredoxins. As a result, the steady state of the probe is governed by the relative kinetics of oxidation and reduction. The additional mechanistic information that is now available on the endogenous reduction via the glutathione pool in the Arabidopsis cytosol and the mitochondrial matrix provides the required framework to interpret sensing data mechanistically and with consideration of the redox context. A similar mechanistic investigation into the H_2O_2 sensing mechanism is only available for the peroxiredoxin-fusion sensor roGFP2-Tsa2 (Morgan *et al.*, 2016), which is only established for yeast. It needs pointing out that peroxynitrite ($ONOO^-$) can show similar reaction behaviour as H_2O_2 with reactive protein thiols (Dubuisson *et al.*, 2004). A recent study found roGFP2-Orp1 to respond to $ONOO^-$ *in vitro*, while the response was absent in the E_{GSH} sensor Grx1-roGFP2 (Müller *et al.*, 2017). In contrast, hypochlorous acid and polysulfides showed reactivity with both sensors. Increased rates of $ONOO^-$ generation may

occur *in planta* via the reaction between NO and superoxide, and plausibly coincide with elevated H_2O_2 generation. As such, $ONOO^-$ cannot be ruled out as potential alternative oxidant when interpreting *in vivo* responses of thiol-based H_2O_2 sensors, such as roGFP2-Orp1 or HyPer.

H_2O_2 measurement in living plant cells using sensors of the HyPer family has been reported in several independent cases so far (Costa *et al.*, 2010; Boisson-Dernier *et al.*, 2013; Hernandez-Barrera *et al.*, 2013; Hernandez-Barrera *et al.*, 2015; Exposito-Rodriguez *et al.*, 2017; Mangano *et al.*, 2017; Rodrigues *et al.*, 2017). The roGFP2-Orp1 circumvents several of the key problems associated with the HyPer sensors. Specifically pH stability of roGFP2-Orp1 had been predicted, based on the pH insensitivity of roGFP2 (Schwarzländer *et al.*, 2008; Albrecht *et al.*, 2011), and is experimentally validated here. The lack of a pH response provides a critical advantage to avoid potential artefacts as well as cumbersome pH controls. This is important due to the linkage between H_2O_2 dynamics and pH in the cell. An example is NADPH oxidase activity, which leads to an intracellular release of protons at NADPH oxidation during extracellular superoxide production. Coincident changes in cell physiological parameters during signalling responses appear to be the rule rather than the exception (Poburko *et al.*, 2011; Behera *et al.*, 2018). For example, shifts in intracellular pH can be significant in plants where dynamic changes in photosynthesis and vacuolar transport rely on changes in pH gradients (Raven & Smith, 1980; Felle, 2001). Particularly strong and sudden pH changes can occur in the matrix of individual mitochondria (Schwarzländer *et al.*, 2012a; Santo-Domingo *et al.*, 2013), which have led to confusion over the usage of different pH-sensitive biosensors (Demaurex & Schwarzländer, 2016). RoGFP2-Orp1 will rule out pH-related ambiguities in interpretation of H_2O_2 sensing data in future studies.

A key insight from our data on roGFP2-Orp1 applies for any dynamic H_2O_2 sensor that detects H_2O_2 by being oxidised in a reversible manner: the steady state of the sensor is generally set by the relative electron fluxes towards and away from the sensor pool. This means that dynamic monitoring specifically of H_2O_2 is only possible under the assumption that the reduction rate remains constant. If so, then changes in sensor oxidation can be linked directly to changes in H_2O_2. This is plausible under many physiological situations of small or moderate H_2O_2 elevations. Once E_{GSH} is also shifted, due to oxidation of GSH to GSSG or due to pool depletion (Meyer *et al.*, 2007; Marty *et al.*, 2009), the redox state of the sensor will follow. This is likely to be the case in the *gr1* and *gr2* mutant backgrounds that we have explored, although increased H_2O_2 flux may occur simultaneously, as indicated by a more oxidised mitochondrial sensor when cytosolic GR1 was absent. From a physiological perspective, the mechanism by which H_2O_2 induces sensor oxidation, i.e. directly or via a shift in E_{GSH}, may be regarded equivalent in many situations, since the signalling outcome for a endogenous transduction protein responsive to H_2O_2/E_{GSH} would be analogous. Changes

in E_{GSH} unrelated to H_2O_2 homeostasis (*e.g.*, pool depletion) may also change the sensor response, however, which needs careful consideration, and can be controlled for (Meyer *et al.*, 2001).

Our data confirm previous theoretical considerations that dynamic H_2O_2 sensors are not suitable to determine absolute intracellular H_2O_2 concentrations (Schwarzländer *et al.*, 2016). Experiments that apply defined external H_2O_2 concentrations and link those to a given intracellular sensor response provide a degree of correlation with external H_2O_2 concentrations in a given system (*e.g.*, Ermakova *et al.*, 2014), but carry little meaning for any H_2O_2 quantification inside the cell. Even cell permeabilisation would not provide any meaningful advantage, since it is the dynamic intracellular equilibrium between oxidation and reduction rates that sets the sensor response and those rates strictly depend on the individual subcellular environment and the physiological conditions.

Consideration of the *in vivo* properties of the sensor now allow detailed interpretation of endogenous H_2O_2 measurements including inference about the passage of H_2O_2 across membranes and its interaction with the local antioxidant systems within a specific cell compartment. We take advantage of the fact that H_2O_2 generation by NADPH oxidases (via superoxide) towards the apoplast is well characterised in plants. This is because extracellular ROS can be detected straightforwardly by extracellular probes and because weaker antioxidant defence extends the half-life of extracellular H_2O_2 (Møller *et al.*, 2007). Luminol-based detection and nitro blue tetrazolium-staining have proven useful to study NADPH oxidase activation in elicitor signalling and development (Jones *et al.*, 2007; Potocky *et al.*, 2007; Kadota *et al.*, 2014). Reliable data for the impact of plasma membrane NADPH oxidase stimulation on intracellular H_2O_2 dynamics are largely lacking, but seem critical if we are to understand the mechanisms to operate in different cell compartments *e.g*. during pathogen defence or guard cell dynamics.

The elicitor measurements demonstrate that RBOH-derived H_2O_2 clearly reaches the cytosol at sufficient rates to oxidise specific cysteine thiols. Influx of H_2O_2 was found to be mediated by *At*PIP1;4 during plant-pathogen interaction and by *At*PIP2;1 in guard cell signalling (Grondin *et al.*, 2015; Tian *et al.*, 2016). H_2O_2 passage via *At*PIP2;1 was recently shown by *ex vivo* HyPer imaging of guard cells in epidermal peels (Rodrigues *et al.*, 2017). The multiwell fluorimetry-based analysis employed here cannot specifically monitor guard cells, but detects fluorescence from all cells of the intact leaf tissue layers, accounts for the recovery after the injury of generating leaf discs (injury has been found to cause oxidation artefacts in epidermal peel preparation; Scuffi *et al.*, 2018) and shows low variability while allowing for parallel measurement of large sample numbers. By making use of genetic backgrounds in which glutathione reduction and/or H_2O_2 detoxification is weakened, the measured H_2O_2 response can be boosted, as evident from the flg22-induced sensor

response amplitude in the WT, *gr1* and *gr2* backgrounds. The technical advantage in monitoring oxidation events that are undetectable in the WT is demonstrated by our experiments, where the chitosan DA 50% response could not be separated from the chitosan DA 0% and the solvent control in the wild type, but showed a clear difference in the *gr1* mutant background.

A recent study using the free roGFP2 in the mitochondrial matrix of Arabidopsis leaves, found a gradient of glutathione oxidation from the penetration side of the non-adapted powdery mildew (Fuchs *et al.*, 2016). Mitochondria close to the penetration site contained a more oxidised glutathione pool than those more distant in the same cell. It was speculated whether local activity of NADPH oxidase by the plant and/or by the fungus may be responsible. Our observation of elicitor-induced sensor oxidation in the cytosol and the mitochondria validates the concept of inter-compartmental H_2O_2 dynamics. While the prolonged oxidation response in the cytosol as compared to the extracellular space may imply intracellular amplification of the H_2O_2 stimulus or a gradual decline of cytosolic antioxidant capacity, the impact of the oxidative burst was hardly detectable in the mitochondrial matrix. That points to passive oxidation in the matrix by H_2O_2 influx under the specific conditions rather than active H_2O_2 production and amplification by the H_2O_2-generating machinery of the organelle itself (Yao *et al.*, 2002; Riemer *et al.*, 2015; Huang *et al.*, 2016). The significance of proximity between a site of pathogen perception and subcellular organelles in intracellular H_2O_2 signalling could not be resolved by the multiwell approach employed here but will lend itself to further exploration by confocal imaging of roGFP2-Orp1 in the future.

Acknowledgements

We thank Bastian Oldenkott (Bonn), Esther Engelhardt (Cologne) and Florian Kotnik (Münster) for assistance with experimental optimisation, and Jörg Kudla for access to the Leica SP5 confocal microscope. This work was supported by the Deutsche Forschungsgemeinschaft (DFG) through the Emmy-Noether programme (SCHW1719/ 1-1), the Research Training Group ('Water use efficiency and drought stress responses: From Arabidopsis to Barley'), the priority program SPP1710 'Dynamics of thiol-based redox switches in cellular physiology' (SCHW1719/ 7-1, ME1567/9-1) and a project grant (SCHW1719/5-1) as part of the package PAK918. The Boost Fund project "PlaMint" of the Bioeconomy Science Center (BioSC) provided partial support. The scientific activities of the Bioeconomy Science Center were financially supported by the Ministry of Innovation, Science and Research within the framework of the NRW Strategieprojekt BioSC No. 313/323-400-002 13.

Author contributions

T.N. and M.S. designed research; T.N., M.E., C.R., J.S., J.M.U., P.F., S.W., L.O., A.M. performed research; P.L., M.D.F., B.M.M., A.C., A.J.M contributed new reagents/plant lines/analytic tools; T.N., M.E., C.R., J.S., P.F., S.W., S.J.M.-S. analysed data and T.N. and M.S. wrote the paper with assistance from all co-authors.

References

Albrecht SC, Barata AG, Grosshans J, Teleman AA, Dick TP. 2011. *In vivo* mapping of hydrogen peroxide and oxidised glutathione reveals chemical and regional specificity of redox homeostasis. *Cell Metabolism* **14**(6): 819-829.

Albrecht SC, Sobotta MC, Bausewein D, Aller I, Hell R, Dick TP, Meyer AJ. 2014. Redesign of genetically encoded biosensors for monitoring mitochondrial redox status in a broad range of model eukaryotes. *Journal of Biomolecular Screening* **19**(3): 379-386.

Behera S, Wang N, Zhang C, Schmitz-Thom I, Strohkamp S, Schultke S, Hashimoto K, Xiong L, Kudla J. 2015. Analyses of Ca^{2+} dynamics using a ubiquitin-10 promoter-driven Yellow Cameleon 3.6 indicator reveal reliable transgene expression and differences in cytoplasmic Ca^{2+} responses in Arabidopsis and rice (*Oryza sativa*) roots. *New Phytologist* **206**(2): 751-760.

Behera S, Z X, Luoni L, Bonza MC, Doccula FG, De Michelis MI, Morris RJ, Schwarzländer M, Costa A. 2018. Cellular Ca^{2+} signals generate defined pH signatures in plants. *Plant Cell.* in press

Belousov VV, Fradkov AF, Lukyanov KA, Staroverov DB, Shakhbazov KS, Terskikh AV, Lukyanov S. 2006. Genetically encoded fluorescent indicator for intracellular hydrogen peroxide. *Nature Methods* **3**(4): 281-286.

Bestetti S, Medrano-Fernandez I, Galli M, Ghitti M, Bienert GP, Musco G, Orsi A, Rubartelli A, Sitia R. 2018. A persulfidation-based mechanism controls aquaporin-8 conductance. *Science advances* **4**(5): eaar5770.

Bienert GP, Chaumont F. 2014. Aquaporin-facilitated transmembrane diffusion of hydrogen peroxide. *Biochim Biophys Acta* **1840**(5): 1596-1604.

Bilan DS, Pase L, Joosen L, Gorokhovatsky AY, Ermakova YG, Gadella TWJ, Grabher C, Schultz C, Lukyanov S, Belousov VV. 2013. HyPer-3: A genetically encoded H_2O_2 probe with improved performance for ratiometric and fluorescence lifetime imaging. *ACS Chemical Biology* **8**(3): 535-542.

Bode M, Longen S, Morgan B, Peleh V, Dick TP, Bihlmaier K, Herrmann JM. 2013. Inaccurately assembled cytochrome *c* oxidase can lead to oxidative stress-induced growth arrest. *Antioxid Redox Signal* **18**(13): 1597-1612.

Boisson-Dernier A, Lituiev DS, Nestorova A, Franck CM, Thirugnanarajah S, Grossniklaus U. 2013. ANXUR receptor-like kinases coordinate cell wall integrity with growth at the pollen tube tip via NADPH oxidases. *PLoS Biol* **11**(11): e1001719.

Buettner GR. 2015. Moving free radical and redox biology ahead in the next decade(s). *Free Radic Biol Med* **78**: 236-238.

Chaouch S, Queval G, Noctor G. 2012. AtRbohF is a crucial modulator of defence-associated metabolism and a key actor in the interplay between intracellular oxidative stress and pathogenesis responses in Arabidopsis. *Plant Journal* **69**(4): 613-627.

Chaudhuri B, Hormann F, Lalonde S, Brady SM, Orlando DA, Benfey P, Frommer WB. 2008. Protonophore- and pH-insensitive glucose and sucrose accumulation detected by FRET nanosensors in Arabidopsis root tips. *Plant Journal* **56**(6): 948-962.

Choudhury FK, Rivero RM, Blumwald E, Mittler R. 2017. Reactive oxygen species, abiotic stress and stress combination. *Plant J* **90**(5): 856-867.

Costa A, Drago I, Behera S, Zottini M, Pizzo P, Schroeder JI, Pozzan T, Lo Schiavo F. 2010. H_2O_2 in plant peroxisomes: an *in vivo* analysis uncovers a Ca^{2+}-dependent scavenging system. *Plant Journal* **62**(5): 760-772.

Daloso DM, Muller K, Obata T, Florian A, Tohge T, Bottcher A, Riondet C, Banat L, Carrari F, Nunes-Nesi A, et al. 2015. Thioredoxin, a master regulator of the tricarboxylic acid cycle in plant mitochondria. *Proc Natl Acad Sci U S A* **112**(11): E1392-E1400.

De Col V, Fuchs P, Nietzel T, Elsasser M, Voon CP, Candeo A, Seeliger I, Fricker MD, Grefen C, Møller IM, et al. 2017. ATP sensing in living plant cells reveals tissue gradients and stress dynamics of energy physiology. *Elife* **6**.

Delaunay A, Pflieger D, Barrault MB, Vinh J, Toledano MB. 2002. A thiol peroxidase is an H_2O_2 receptor and redox-transducer in gene activation. *Cell* **111**(4): 471-481.

Demaurex N, Schwarzländer M. 2016. Mitochondrial flashes: dump superoxide and dance with protons now. *Antioxid Redox Signal* **25**(9): 550-551.

Deuschle K, Chaudhuri B, Okumoto S, Lager I, Lalonde S, Frommer WB. 2006. Rapid metabolism of glucose detected with FRET glucose nanosensors in epidermal cells and intact roots of Arabidopsis RNA-silencing mutants. *Plant Cell* **18**(9): 2314-2325.

Devireddy AR, Zandalinas SI, Gomez-Cadenas A, Blumwald E, Mittler R. 2018. Coordinating the overall stomatal response of plants: rapid leaf-to-leaf communication during light stress. *Sci Signal* **11**(518).

Dikalov S. 2011. Cross talk between mitochondria and NADPH oxidases. *Free Radical Biology and Medicine* **51**(7): 1289-1301.

Dooley CT, Dore TM, Hanson GT, Jackson WC, Remington SJ, Tsien RY. 2004. Imaging dynamic redox changes in mammalian cells with green fluorescent protein indicators. *Journal of Biological Chemistry* **279**(21): 22284-22293.

Dubuisson M, Vander Stricht D, Clippe A, Etienne F, Nauser T, Kissner R, Koppenol WH, Rees JF, Knoops B. 2004. Human peroxiredoxin 5 is a peroxynitrite reductase. *FEBS Lett* **571**(1-3): 161-165.

El Zawily AM, Schwarzländer M, Finkemeier I, Johnston IG, Benamar A, Cao Y, Gissot C, Meyer AJ, Wilson K, Datla R, et al. 2014. FRIENDLY regulates mitochondrial distribution, fusion, and quality control in Arabidopsis. *Plant Physiol* **166**(2): 808-828.

Ermakova YG, Bilan DS, Matlashov ME, Mishina NM, Markvicheva KN, Subach OM, Subach FV, Bogeski I, Hoth M, Enikolopov G, et al. 2014. Red fluorescent genetically encoded indicator for intracellular hydrogen peroxide. *Nat Commun* **5**: 5222.

Exposito-Rodriguez M, Laissue PP, Littlejohn GR, Smirnoff N, Mullineaux PM. 2013. The use of HyPer to examine spatial and temporal changes in H_2O_2 in high light-exposed plants. *Methods Enzymol* **527**: 185-201.

Exposito-Rodriguez M, Laissue PP, Yvon-Durocher G, Smirnoff N, Mullineaux PM. 2017. Photosynthesis-dependent H_2O_2 transfer from chloroplasts to nuclei provides a high-light signalling mechanism. *Nat Commun* **8**(1): 49.

Ezerina D, Morgan B, Dick TP. 2014. Imaging dynamic redox processes with genetically encoded probes. *J Mol Cell Cardiol* **73**: 43-49.

Felle HH. 2001. pH: Signal and messenger in plant cells. *Plant Biology* **3**(6): 577-591.

Finkemeier I, Goodman M, Lamkemeyer P, Kandlbinder A, Sweetlove LJ, Dietz KJ. 2005. The mitochondrial type II peroxiredoxin F is essential for redox homeostasis and root growth of *Arabidopsis thaliana* under stress. *Journal of Biological Chemistry* **280**(13): 12168-12180.

Foreman J, Demidchik V, Bothwell JHF, Mylona P, Miedema H, Torres MA, Linstead P, Costa S, Brownlee C, Jones JDG, et al. 2003. Reactive oxygen species produced by NADPH oxidase regulate plant cell growth. *Nature* **422**(6930): 442-446.

Fricker MD. 2016. Quantitative redox imaging software. *Antioxid Redox Signal* **24**(13): 752-762.

Fuchs R, Kopischke M, Klapprodt C, Hause G, Meyer AJ, Schwarzländer M, Fricker MD, Lipka V. 2016. Immobilized subpopulations of leaf epidermal mitochondria mediate PENETRATION2-dependent pathogen entry control in Arabidopsis. *Plant Cell* **28**(1): 130-145.

Gelhaye E, Rouhier N, Gerard J, Jolivet Y, Gualberto J, Navrot N, Ohlsson PI, Wingsle G, Hirasawa M, Knaff DB, et al. 2004. A specific form of thioredoxin h occurs in plant mitochondria and regulates the alternative oxidase. *Proc Natl Acad Sci U S A* **101**(40): 14545-14550.

Giacomelli L, Masi A, Ripoll DR, Lee MJ, van Wijk KJ. 2007. *Arabidopsis thaliana* deficient in two chloroplast ascorbate peroxidases shows accelerated light-induced necrosis when levels of cellular ascorbate are low. *Plant Mol Biol* **65**(5): 627-644.

Gomes A, Fernandes E, Lima JLFC. 2005. Fluorescence probes used for detection of reactive oxygen species. *Journal of Biochemical and Biophysical Methods* **65**(2-3): 45-80.

Grant JJ, Yun BW, Loake GJ. 2000. Oxidative burst and cognate redox signalling reported by luciferase imaging: identification of a signal network that functions independently of ethylene, SA and Me-JA but is dependent on MAPKK activity. *Plant Journal* **24**(5): 569-582.

Grondin A, Rodrigues O, Verdoucq L, Merlot S, Leonhardt N, Maurel C. 2015. Aquaporins contribute to ABA-triggered stomatal closure through OST1-mediated phosphorylation. *Plant Cell* **27**(7): 1945-1954.

Gubaeva E, Gubaev A, Melcher R, Cord-Landwehr S, Singh R, El Gueddari NE, Moerschbacher BM. 2018. 'Slipped sandwich' model for chitin and chitosan perception in Arabidopsis. *Molecular Plant Microbe Interactions*. doi: 10.1094/MPMI-04-18-0098-R.

Gutscher M, Pauleau AL, Marty L, Brach T, Wabnitz GH, Samstag Y, Meyer AJ, Dick TP. 2008. Real-time imaging of the intracellular glutathione redox potential. *Nature Methods* **5**(6): 553-559.

Gutscher M, Sobotta MC, Wabnitz GH, Ballikaya S, Meyer AJ, Samstag Y, Dick TP. 2009. Proximity-based protein thiol oxidation by H_2O_2-scavenging peroxidases. *Journal of Biological Chemistry* **284**(46): 31532-31540.

Hanson GT, Aggeler R, Oglesbee D, Cannon M, Capaldi RA, Tsien RY, Remington SJ. 2004. Investigating mitochondrial redox potential with redox-sensitive green fluorescent protein indicators. *Journal of Biological Chemistry* **279**(13): 13044-13053.

Hernandez-Barrera A, Quinto C, Johnson EA, Wu HM, Cheung AY, Cardenas L. 2013. Using hyper as a molecular probe to visualize hydrogen peroxide in living plant cells: a method with virtually unlimited potential in plant biology. *Methods Enzymol* **527**: 275-290.

Hernandez-Barrera A, Velarde-Buendia A, Zepeda I, Sanchez F, Quinto C, Sanchez-Lopez R, Cheung AY, Wu HM, Cardenas L. 2015. Hyper, a hydrogen peroxide

sensor, indicates the sensitivity of the Arabidopsis root elongation zone to aluminum treatment. *Sensors (Basel)* **15**(1): 855-867.

Huang S, Van Aken O, Schwarzländer M, Belt K, Millar AH. 2016. The roles of mitochondrial reactive oxygen species in cellular signaling and stress response in plants. *Plant Physiol* **171**(3): 1551-1559.

Jones AM, Danielson JA, Manojkumar SN, Lanquar V, Grossmann G, Frommer WB. 2014. Abscisic acid dynamics in roots detected with genetically encoded FRET sensors. *Elife* **3**: e01741.

Jones MA, Raymond MJ, Yang Z, Smirnoff N. 2007. NADPH oxidase-dependent reactive oxygen species formation required for root hair growth depends on ROP GTPase. *J Exp Bot* **58**(6): 1261-1270.

Kadota Y, Sklenar J, Derbyshire P, Stransfeld L, Asai S, Ntoukakis V, Jones JD, Shirasu K, Menke F, Jones A, et al. 2014. Direct regulation of the NADPH oxidase RBOHD by the PRR-associated kinase BIK1 during plant immunity. *Mol Cell* **54**(1): 43-55.

Kerchev P, Waszczak C, Lewandowska A, Willems P, Shapiguzov A, Li Z, Alseekh S, Muhlenbock P, Hoeberichts FA, Huang J, et al. 2016. Lack of GLYCOLATE OXIDASE1, but not GLYCOLATE OXIDASE2, attenuates the photorespiratory phenotype of CATALASE2-deficient Arabidopsis. *Plant Physiol* **171**(3): 1704-1719.

Kwak JM, Mori IC, Pei ZM, Leonhardt N, Torres MA, Dangl JL, Bloom RE, Bodde S, Jones JD, Schroeder JI. 2003. NADPH oxidase AtrbohD and AtrbohF genes function in ROS-dependent ABA signaling in Arabidopsis. *EMBO J* **22**(11): 2623-2633.

Laloi C, Rayapuram N, Chartier Y, Grienenberger JM, Bonnard G, Meyer Y. 2001. Identification and characterization of a mitochondrial thioredoxin system in plants. *Proc Natl Acad Sci U S A* **98**(24): 14144-14149.

Langford TF, Huang BK, Lim JB, Moon SJ, Sikes HD. 2018. Monitoring the action of redox-directed cancer therapeutics using a human peroxiredoxin-2-based probe. *Nat Commun* **9**(1): 3145.

Lassig R, Gutermuth T, Bey TD, Konrad KR, Romeis T. 2014. Pollen tube NAD(P)H oxidases act as a speed control to dampen growth rate oscillations during polarized cell growth. *Plant J* **78**(1): 94-106.

Lee Y, Rubio MC, Alassimone J, Geldner N. 2013. A mechanism for localized lignin deposition in the endodermis. *Cell* **153**(2): 402-412.

Lee Y, Yoon TH, Lee J, Jeon SY, Lee JH, Lee MK, Chen H, Yun J, Oh SY, Wen X, et al. 2018. A lignin molecular brace controls precision processing of cell walls critical for surface integrity in Arabidopsis. *Cell* **173**(6): 1468-1480 e1469.

Lehmann M, Schwarzländer M, Obata T, Sirikantaramas S, Burow M, Olsen CE, Tohge T, Fricker MD, Møller BL, Fernie AR, et al. 2009. The metabolic response of Arabidopsis roots to oxidative stress is distinct from that of heterotrophic cells in culture and highlights a complex relationship between the levels of transcripts, metabolites, and flux. *Mol Plant* **2**(3): 390-406.

Loro G, Wagner S, Doccula FG, Behera S, Weinl S, Kudla J, Schwarzländer M, Costa A, Zottini M. 2016. Chloroplast-specific *in vivo* Ca^{2+} imaging using Yellow Cameleon fluorescent protein sensors reveals organelle-autonomous Ca^{2+} signatures in the stroma. *Plant Physiol* **171**(4): 2317-2330.

Mangano S, Denita-Juarez SP, Choi HS, Marzol E, Hwang Y, Ranocha P, Velasquez SM, Borassi C, Barberini ML, Aptekmann AA, et al. 2017. Molecular link between auxin and ROS-mediated polar growth. *Proc Natl Acad Sci U S A* **114**(20): 5289-5294.

Marchesi E, Rota C, Fann YC, Chignell CF, Mason RP. 1999. Photoreduction of the fluorescent dye 2',7'-dichlorofluorescein: A spin trapping and direct electron spin resonance study with implications for oxidative stress measurements. *Free Radical Biology and Medicine* **26**(1-2): 148-161.

Markvicheva KN, Bilan DS, Mishina NM, Gorokhovatsky AY, Vinokurov LM, Lukyanov S, Belousov VV. 2011. A genetically encoded sensor for H_2O_2 with expanded dynamic range. *Bioorganic & Medicinal Chemistry* **19**(3): 1079-1084.

Marty L, Siala W, Schwarzländer M, Fricker MD, Wirtz M, Sweetlove LJ, Meyer Y, Meyer AJ, Reichheld JP, Hell R. 2009. The NADPH-dependent thioredoxin system constitutes a functional backup for cytosolic glutathione reductase in Arabidopsis. *Proc Natl Acad Sci U S A* **106**(22): 9109-9114.

Matlashov ME, Bogdanova YA, Ermakova GV, Mishina NM, Ermakova YG, Nikitin ES, Balaban PM, Okabe S, Lukyanov S, Enikolopov G, et al. 2015. Fluorescent ratiometric pH indicator SypHer2: Applications in neuroscience and regenerative biology. *Biochim Biophys Acta* **1850**(11): 2318-2328.

Melcher RL, Moerschbacher BM. 2016. An improved microtiter plate assay to monitor the oxidative burst in monocot and dicot plant cell suspension cultures. *Plant Methods* **12**: 5.

Meyer AJ, Brach T, Marty L, Kreye S, Rouhier N, Jacquot JP, Hell R. 2007. Redox-sensitive GFP in *Arabidopsis thaliana* is a quantitative biosensor for the redox potential of the cellular glutathione redox buffer. *Plant Journal* **52**(5): 973-986.

Meyer AJ, May MJ, Fricker M. 2001. Quantitative *in vivo* measurement of glutathione in Arabidopsis cells. *Plant Journal* **27**(1): 67-78.

Meyer AJ, Riemer J, Rouhier N. 2018. Oxidative protein folding: state-of-the-art and current avenues of research in plants. *New Phytologist.* doi: 10.1111/nph.15436

Miller G, Schlauch K, Tam R, Cortes D, Torres MA, Shulaev V, Dangl JL, Mittler R. 2009. The plant NADPH oxidase RBOHD mediates rapid systemic signaling in response to diverse stimuli. *Sci Signal* **2**(84): ra45.

Møller IM, Jensen PE, Hansson A. 2007. Oxidative modifications to cellular components in plants. *Annu Rev Plant Biol* **58**: 459-481.

Morgan B, Van Laer K, Owusu TNE, Ezerina D, Pastor-Flores D, Amponsah PS, Tursch A, Dick TP. 2016. Real-time monitoring of basal H_2O_2 levels with peroxiredoxin-based probes. *Nat Chem Biol* **12**(6): 437-U495.

Müller A, Schneider JF, Degrossoli A, Lupilova N, Dick TP, Leichert LI. 2017. Systematic *in vitro* assessment of responses of roGFP2-based probes to physiologically relevant oxidant species. *Free Radic Biol Med* **106**: 329-338.

Ortega-Villasante C, Buren S, Blazquez-Castro A, Baron-Sola A, Hernandez LE. 2018. Fluorescent *in vivo* imaging of reactive oxygen species and redox potential in plants. *Free Radical Biology and Medicine*. **122**: 202-220.

Pei ZM, Murata Y, Benning G, Thomine S, Klusener B, Allen GJ, Grill E, Schroeder JI. 2000. Calcium channels activated by hydrogen peroxide mediate abscisic acid signalling in guard cells. *Nature* **406**(6797): 731-734.

Peralta D, Bronowska AK, Morgan B, Doka E, Van Laer K, Nagy P, Grater F, Dick TP. 2015. A proton relay enhances H_2O_2 sensitivity of GAPDH to facilitate metabolic adaptation. *Nat Chem Biol* **11**(2): 156-163.

Poburko D, Santo-Domingo J, Demaurex N. 2011. Dynamic regulation of the mitochondrial proton gradient during cytosolic calcium elevations. *Journal of Biological Chemistry* **286**(13): 11672-11684.

Potocky M, Jones MA, Bezvoda R, Smirnoff N, Zarsky V. 2007. Reactive oxygen species produced by NADPH oxidase are involved in pollen tube growth. *New Phytologist* **174**(4): 742-751.

Queval G, Issakidis-Bourguet E, Hoeberichts FA, Vandorpe M, Gakiere B, Vanacker H, Miginiac-Maslow M, Van Breusegem F, Noctor G. 2007. Conditional oxidative stress responses in the Arabidopsis photorespiratory mutant *cat2* demonstrate that redox state is a key modulator of daylength-dependent gene expression, and define photoperiod as a crucial factor in the regulation of H_2O_2-induced cell death. *Plant Journal* **52**(4): 640-657.

Ratjens S, Mortensen S, Kumpf A, Bartsch M, Winkelmann T. 2018. Embryogenic callus as target for efficient transformation of *Cyclamen persicum* enabling gene function studies. *Front Plant Sci* **9**: 1035.

Raven JA, Smith FA. 1980. Intracellular pH regulation of the giant-celled marine alga *Chaetomorpha darwinii*. *Journal of Experimental Botany* **31**(124): 1357-1369.

Reichheld JP, Khafif M, Riondet C, Droux M, Bonnard G, Meyer Y. 2007. Inactivation of thioredoxin reductases reveals a complex interplay between thioredoxin and glutathione pathways in Arabidopsis development. *Plant Cell* **19**(6): 1851-1865.

Rezende F, Brandes RP, Schroder K. 2018. Detection of hydrogen peroxide with fluorescent dyes. *Antioxid Redox Signal* **29**(6): 585-602.

Riemer J, Schwarzländer M, Conrad M, Herrmann JM. 2015. Thiol switches in mitochondria: operation and physiological relevance. *Biol Chem* **396**(5): 465-482.

Rodrigues O, Reshetnyak G, Grondin A, Saijo Y, Leonhardt N, Maurel C, Verdoucq L. 2017. Aquaporins facilitate hydrogen peroxide entry into guard cells to mediate ABA- and pathogen-triggered stomatal closure. *Proc Natl Acad Sci U S A* **114**(34): 9200-9205.

Roma LP, Duprez J, Takahashi HK, Gilon P, Wiederkehr A, Jonas JC. 2012. Dynamic measurements of mitochondrial hydrogen peroxide concentration and glutathione redox state in rat pancreatic beta-cells using ratiometric fluorescent proteins: confounding effects of pH with HyPer but not roGFP1. *Biochemical Journal* **441**(3): 971-978.

Santo-Domingo J, Giacomello M, Poburko D, Scorrano L, Demaurex N. 2013. OPA1 promotes pH flashes that spread between contiguous mitochondria without matrix protein exchange. *EMBO J* **32**(13): 1927-1940.

Schwarzländer M, Dick TP, Meyer AJ, Morgan B. 2016. Dissecting redox biology using fluorescent protein sensors. *Antioxid Redox Signal* **24**(13): 680-712.

Schwarzländer M, Fricker MD, Muller C, Marty L, Brach T, Novak J, Sweetlove LJ, Hell R, Meyer AJ. 2008. Confocal imaging of glutathione redox potential in living plant cells. *Journal of Microscopy* **231**(2): 299-316.

Schwarzländer M, Logan DC, Johnston IG, Jones NS, Meyer AJ, Fricker MD, Sweetlove LJ. 2012a. Pulsing of membrane potential in individual mitochondria: a stress-induced mechanism to regulate respiratory bioenergetics in Arabidopsis. *Plant Cell* **24**(3): 1188-1201.

Schwarzländer M, Murphy MP, Duchen MR, Logan DC, Fricker MD, Halestrap AP, Muller FL, Rizzuto R, Dick TP, Meyer AJ, et al. 2012b. Mitochondrial 'flashes': a radical concept repHined. *Trends Cell Biol* **22**(10): 503-508.

Schwarzländer M, Wagner S, Ermakova YG, Belousov VV, Radi R, Beckman JS, Buettner GR, Demaurex N, Duchen MR, Forman HJ, et al. 2014. The 'mitoflash' probe cpYFP does not respond to superoxide. *Nature* **514**(7523): E12-E14.

Scuffi D, Nietzel T, Di Fino LM, Meyer AJ, Lamattina L, Schwarzländer M, Laxalt AM, Garcia-Mata C. 2018. Hydrogen sulfide increases production of NADPH oxidase-dependent hydrogen peroxide and phospholipase D-derived phosphatidic acid in guard cell signaling. *Plant Physiol* **176**(3): 2532-2542.

Siddique S, Matera C, Radakovic ZS, Hasan MS, Gutbrod P, Rozanska E, Sobczak M, Torres MA, Grundler FM. 2014. Parasitic worms stimulate host NADPH oxidases to produce reactive oxygen species that limit plant cell death and promote infection. *Sci Signal* **7**(320): ra33.

Sierla M, Waszczak C, Vahisalu T, Kangasjarvi J. 2016. Reactive oxygen species in the regulation of stomatal movements. *Plant Physiol* **171**(3): 1569-1580.

Smirnoff N, Arnaud D. 2018. Hydrogen peroxide metabolism and functions in plants. *New Phytologist.* doi: 10.1111/nph.15488

Sobotta MC, Barata AG, Schmidt U, Mueller S, Millonig G, Dick TP. 2013. Exposing cells to H_2O_2: a quantitative comparison between continuous low-dose and one-time high-dose treatments. *Free Radical Biology and Medicine* **60**: 325-335.

Sobotta MC, Liou W, Stocker S, Talwar D, Oehler M, Ruppert T, Scharf AN, Dick TP. 2015. Peroxiredoxin-2 and STAT3 form a redox relay for H_2O_2 signaling. *Nat Chem Biol* **11**(1): 64-70.

Tian S, Wang X, Li P, Wang H, Ji H, Xie J, Qiu Q, Shen D, Dong H. 2016. Plant aquaporin *At*PIP1;4 links apoplastic H_2O_2 induction to disease immunity pathways. *Plant Physiol* **171**(3): 1635-1650.

Veal EA, Day AM, Morgan BA. 2007. Hydrogen peroxide sensing and signaling. *Mol Cell* **26**(1): 1-14.

Wagner S, Nietzel T, Aller I, Costa A, Fricker MD, Meyer AJ, Schwarzländer M. 2015. Analysis of plant mitochondrial function using fluorescent protein sensors. *Methods in Molecular Biology* **1305**: 241-252.

Waszczak C, Carmody M, Kangasjarvi J. 2018. Reactive oxygen species in plant signaling. *Annu Rev Plant Biol* **69**: 209-236.

Weerapana E, Wang C, Simon GM, Richter F, Khare S, Dillon MB, Bachovchin DA, Mowen K, Baker D, Cravatt BF. 2010. Quantitative reactivity profiling predicts functional cysteines in proteomes. *Nature* **468**(7325): 790-795.

Weller J, Kizina KM, Can K, Bao G, Muller M. 2014. Response properties of the genetically encoded optical H_2O_2 sensor HyPer. *Free Radical Biology and Medicine* **76**: 227-241.

Yao N, Tada Y, Sakamoto M, Nakayashiki H, Park P, Tosa Y, Mayama S. 2002. Mitochondrial oxidative burst involved in apoptotic response in oats. *Plant Journal* **30**(5): 567-579.

Zheng M, Aslund F, Storz G. 1998. Activation of the OxyR transcription factor by reversible disulfide bond formation. *Science* **279**(5357): 1718-1721.

The following Supporting Information is available for this article:

Fig. S1: Purification of heterologous roGFP2-Orp1 protein, emission spectra and H_2O_2-dependent oxidation rates.

Fig. S2: Analysis of cytosolic roGFP2-Orp1 redox state in different Arabidopsis seedling tissues.

Fig. S3: Redox responses of independent roGFP2-Orp1 Arabidopsis lines and *in planta* spectra of reduced mitochondrial sensor.

Fig. S4: Expression of the fluorescent probe cyt-roGFP2-Orp1 in Arabidopsis.

Fig. S5: Redox response of 2′,7′-dichlorodihydrofluorescin diacetate and mt-roGFP2-Orp1 in Arabidopsis seedlings to menadione.

Fig. S6: The response of cyt-roGFP2-Orp1 to flg22-triggered oxidative burst in diphenyleneiodonium-treated Arabidopsis leaf discs.

Table S1: Primer sequences for cloning of the expression vectors.

Methods S1: Cloning of sensor constructs and generation of plant lines.

Methods S2: Plant culture.

Methods S3: Purification of roGFP2-Orp1 protein.

Methods S4: Elicitors.

Figures Legends

Fig. 1: Expression of roGFP2-Orp1 in Arabidopsis. (**a)** A model of the biochemical mechanisms by which roGFP2-Orp1 responds reversibly to changes in H_2O_2, including a proximity-based redox relay between the cysteines of roGFP2 and Orp1 (Gutscher *et al.*, 2009). Red arrows indicate nucleophilic attack. (**b**) Subcellular localisation of cyt-roGFP2-Orp1 in cotyledon epidermal cells of 5-day-old Arabidopsis seedlings (excitation: 488 nm; emission: 520 ± 15 nm for roGFP2-Orp1 and 675 ± 25 nm for chlorophyll). The overlay shows roGFP2-Orp1 and the bright field image. Bar: 20 µm. (**c**) Subcellular localisation of mt-roGFP2-Orp1 in root epidermal cells of 5-day-old Arabidopsis seedlings (excitation: 488 nm, emission: 520 ± 15 nm for roGFP2-Orp1; excitation: 543 nm, emission: 595 ± 25 nm for MitoTracker Orange CMTMRos). The overlay shows roGFP2-Orp1 and the MitoTracker fluorescence. Bar: 10 µm. (**d**) Rosettes of 27-day-old Arabidopsis plants of two independent

cytosolic (cyt-roGFP2-Orp1) and two mitochondrial (mt-roGFP2-Orp1) sensor lines grown side-by-side with the corresponding wild type, Col-0. Bar: 4 cm.

Fig. 2: *In vitro* characteristics of roGFP2-Orp1. (**a**) The excitation spectra of purified roGFP2-Orp1 sensor protein (*n*=4 technical replicates; error bars: ±SD; excitation: 1 nm steps with 5 nm bandwidth; emission: 515 ± 2.5 nm). RoGFP2-Orp1 was oxidised or reduced by addition of 2,2-dithiopyridylsulfide (DPS, 1 mM) or dithiothreitol (DTT, 20 mM), respectively. The spectroscopic dynamic range (δ) was calculated from the 405 nm/488 nm excitation ratios for the oxidised and reduced probe. (**b**) The pH-sensitivity of roGFP2-Orp1 was analysed *in vitro*. The fluorescence ratios (*n*=3 technical replicates; vertical error bars: ±SD, but not visible; sequential excitation: 400 ± 5 nm and 482 ± 8 nm; emission: 520 ± 5 nm) in the pH range of 5.3-8.3 are shown. The pH of the buffer (MES-KOH for pH 5.3-6.5; HEPES-KOH for pH 7-8 and Tris-HCl for pH 8.1-8.3) was controlled with a pH mini-electrode (*n*=3 technical replicates; horizontal error bars: ±SD). The dynamic range ($\delta_{400\ nm/482\ nm}$) is plotted on the secondary axis. (**c**) Superoxide dismutates to H_2O_2 either spontaneously or by superoxide dismutase (SOD) catalysis. H_2O_2 triggers the reversible oxidation of roGFP2-Orp1. Oxidised roGFP2-Orp1 is reduced either by thioredoxin (TRX) / NADPH-dependent thioredoxin reductase (NTR) or by the glutaredoxin (GRX) / glutathione (GSH) / glutathione reductase (GR) system. Both pathways obtain their electrons from the oxidation of NADPH, which is provided by the metabolism. (**d**) Pre-reduced roGFP2-Orp1 (20 mM DTT for 20 min on ice followed by depletion of excess DTT using a protein desalting column) was titrated with different amounts of H_2O_2. The fluorescence ratios (sequential excitation: 400 ± 5 nm and 482 ± 8 nm; emission: 520 ± 5 nm; normalised to the highest value) of roGFP2-Orp1 (0.3 µM) are detected over time. First arrow indicates time point of addition of H_2O_2 to a final concentration of 0 µM, 0.1 µM (1:3 ratio), 0.25 µM (0.83:1 ratio), 1 µM (3.33:1 ratio), 10 µM (33.3:1 ratio). Second arrow indicates timepoint of reduction of the probe (20 mM DTT). Upper dashed line indicates the oxidised state, lower dashed line the reduced state of roGFP2-Orp1. (**e**) The reduction of oxidised roGFP2-Orp1 by the different cellular redox machineries reconstituted *in vitro*. Fluorescence ratios (*n*=3 technical replicates; error bars: ±SD; sequential excitation: 400 ± 5 nm and 482 ± 8 nm; emission: 520 ± 5 nm; mean normalised to the highest value) of roGFP2-Orp1 are plotted over time. The arrow indicates time point of addition thioredoxin-O1 (TRX) and NADPH-dependent thioredoxin reductase b (NTR) for reconstitution of the thioredoxin redox machinery, or of glutathione (10 mM GSH) in the presence of glutathione reductase (GR), or in the presence of GR and glutaredoxin C1 (GRX). NADPH (0.1 mM) was present in all reactions as electron source.

Fig. 3: Cytosolic roGFP2-Orp1 redox state in Arabidopsis seedlings. (**a**) The oxidation state of cytosolic roGFP2-Orp1 is shown for a representative 5-day-old seedling in false colour images (sequential excitation: 405 nm and 488 nm; emission: 520 ± 15 nm). Enlarged are I: cotyledon, II: hypocotyl, III: shoot-root transition zone and IV: root tip. Bar: 1 mm. (**b**) Representative false colour images of root tips of 5-day-old seedlings show the oxidation state of roGFP2-Orp1 targeted either to the cytosol or the mitochondrial matrix. Bar: 50 µm. (**c**) Sensor steady state oxidation levels of root tips of 5-day-old seedlings ($n \geq 8$; boxplots show 10-90% percentiles; outliers indicated as black dots; means indicated by black crosses; significantly different with **p≤0.01, ***p≤0.001 by two-tailed, unpaired Student`s *t*-test) were monitored under physiological conditions and after calibration by the addition of 20 mM DTT or 100 mM H_2O_2. The *in vivo* spectroscopic dynamic range (δ) was calculated from the 405 nm/488 nm excitation ratios for the oxidised and reduced probe.

Fig. 4: RoGFP2-Orp1 redox dynamics in Arabidopsis seedlings treated with menadione. (**a, b**) Excitation spectra of 7-day-old cytosolic (**a**) and mitochondrial (**b**) roGFP-Orp1 seedlings with the corresponding wild type (n=3-5; error bars: ±SD; excitation: 1 nm steps with 10 nm bandwidth; emission: 520 ± 5 nm). (**c**) Excitation spectra of cytosolic roGFP2-Orp1 seedlings following application of 30 µM menadione for 30 min (exemplary excitation scans corrected for auto-fluorescence of Col-0 seedlings). (**d**) The response of cytosolic roGFP2-Orp1 over time (n=3; error bars: ±SD; sequential excitation: 400 ± 5 nm and 482 ± 8 nm; emission: 520 ± 5 nm; means corrected for auto-fluorescence of Col-0 seedlings). Arrow indicates menadione application. The experiments were repeated at least twice with consistent results.

Fig. 5: Redox-state of cytosolic and mitochondrial roGFP2-Orp1 in different mutants of the (thiol) redox systems. (**a**) Mutants impaired at different positions of the redox machinery as used in the analysis; a schematic overview of the localisation of the affected proteins is shown: glutathione reductase 1 (GR1), glutathione reductase 2 (GR2), thioredoxin-O1 (TRX-O1), NADPH-dependent thioredoxin reductase A and B (NTRA/B), catalase-2 (CAT2), stromal ascorbate peroxidase (sAPX) and peroxiredoxin-II F (PRXII F). Four different tissues of 5-day-old Arabidopsis plants were analysed by confocal microscopy, I: cotyledons, II: hypocotyl, III: roots and IV: root tips, as indicated by white boxes on the representative fluorescent seedling. (**b**) Steady state roGFP2-Orp1 oxidation is plotted ($n \geq 6$; sequential excitation: 405 nm and 488 nm; emission: 520 ± 15 nm; boxplots show 10-90% percentiles; outliers indicated as black dots; means indicated by black crosses with * p≤0.05, ** p≤0.01, ***p≤0.001, ****p≤0.0001 with two-way ANOVA and Dunnett's multiple comparisons test) for the cytosolic and the mitochondrial sensors in the different tissues of

the respective mutant backgrounds. For statistical testing Col-0 was compared with all individual mutants within one seedling area but mutants were not compared with each other. (**c**) Cytosolic roGFP2-Orp1 oxidation was monitored in real time in Col-0 seedlings and in *gr1* background by multiwell fluorimetry (*n*=3-4; error bars: ±SD; sequential excitation: 400 ± 5 nm and 482 ± 8 nm; emission: 520 ± 5 nm; means corrected for auto-fluorescence of Col-0 seedlings). H_2O_2 was added where indicated by black arrows (1st addition: 1 mM, 2nd addition: 1 mM, 3rd addition: 5 mM). The differences between control and treatment were significant ($p<0.05$) after minute 174 for Col-0 and after minute 13.5 for *gr1* (considering data points from start of the first treatment minute 10 to 225; *t*-test corrected for multiple comparisons by the Bonferroni-Sidak method). The experiment was repeated twice with consistent results.

Fig. 6: The intracellular responses of roGFP2-Orp1 to elicitor-triggered oxidative burst in Arabidopsis leaf discs. (**a**) Cytosolic roGFP2-Orp1 oxidation was monitored in real time in leaf discs of 4-week-old plants of Col-0 by multiwell fluorimetry (*n*=5; error bars: +SD; sequential excitation: 400 ± 5 nm and 482 ± 8 nm; emission: 520 ± 5 nm; means corrected for auto-fluorescence of Col-0 seedlings). Elicitors were added to a final concentration of 10 µM for flagellin 22 (flg22) and to 0.01 mg/ml for both chitosans, either 50% acetylated (chit. DA50) or 0% acetylated (chit. DA0), as indicated by a black arrow. Inset shows cytosolic roGFP2-Orp1 oxidation in leaf discs pre-incubated with diphenyleneiodonium (DPI, 50 µM) after 100 min of the addition of flg22 (*n*=4; error bars: +SD; sequential excitation: 400 ± 5 nm and 482 ± 8 nm; emission: 520 ± 5 nm; means corrected for auto-fluorescence of Col-0 seedlings with *p≤0.05 by two-tailed, unpaired Student`s *t*-test; full time series in **Supporting Information Figure S6**). (**b**) Luminescence triggered by the different elicitors in a luminol assay (*n*=4; error bars: +SD). (**c**) As in (**a**), but with *gr1* mutant. (**d**) Cyt-roGFP2-Orp1 oxidation 100 min after starting the assay (boxplots show 10-90% percentiles; means indicated by black crosses with a: p>0.05, b: p≤0.05, e: p≤0.0001 with two-way ANOVA and Dunnett's multiple comparisons test). (**e**) As in (**a**) and (**c**), but with mitochondrial roGFP2-Orp1 in Col-0 and *gr2* background and with flg22 only (*n*=5; error bars: +SD; sequential excitation: 400 ± 5 nm and 482 ± 8 nm; emission: 520 ± 5 nm; means corrected for auto-fluorescence of Col-0 seedlings). Red box highlights the initial sensor response in *gr2* background to flg22 treatment. All experiments were repeated at least three times with consistent results. (**f**) Simplified model of the NADPH-oxidase (RBOH)-dependent generation of superoxide, which dismutases to H_2O_2 as detectable in the extracellular space. Entry into the cytosol and the mitochondrial matrix, as well as signal modulation, can be monitored by roGFP2-Orp1.

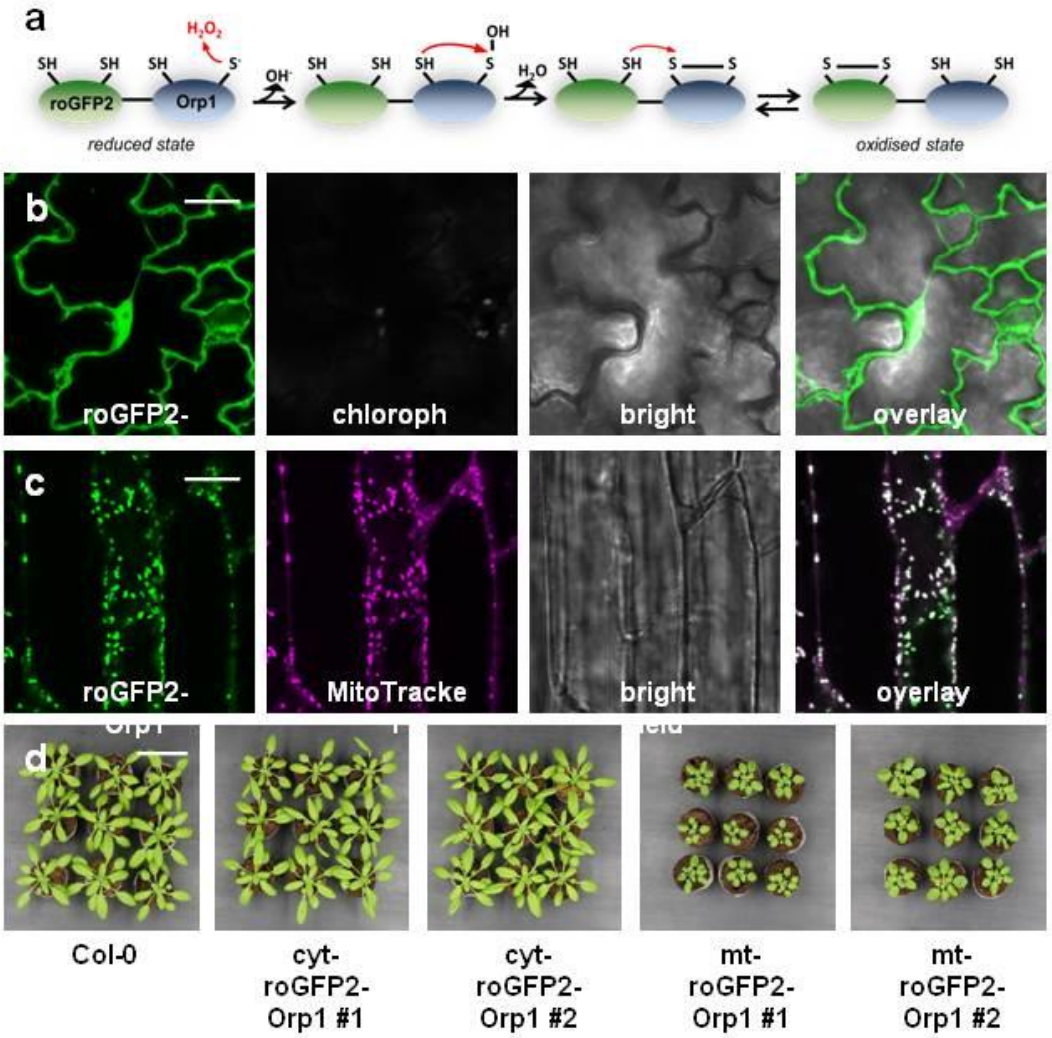

Figure 1

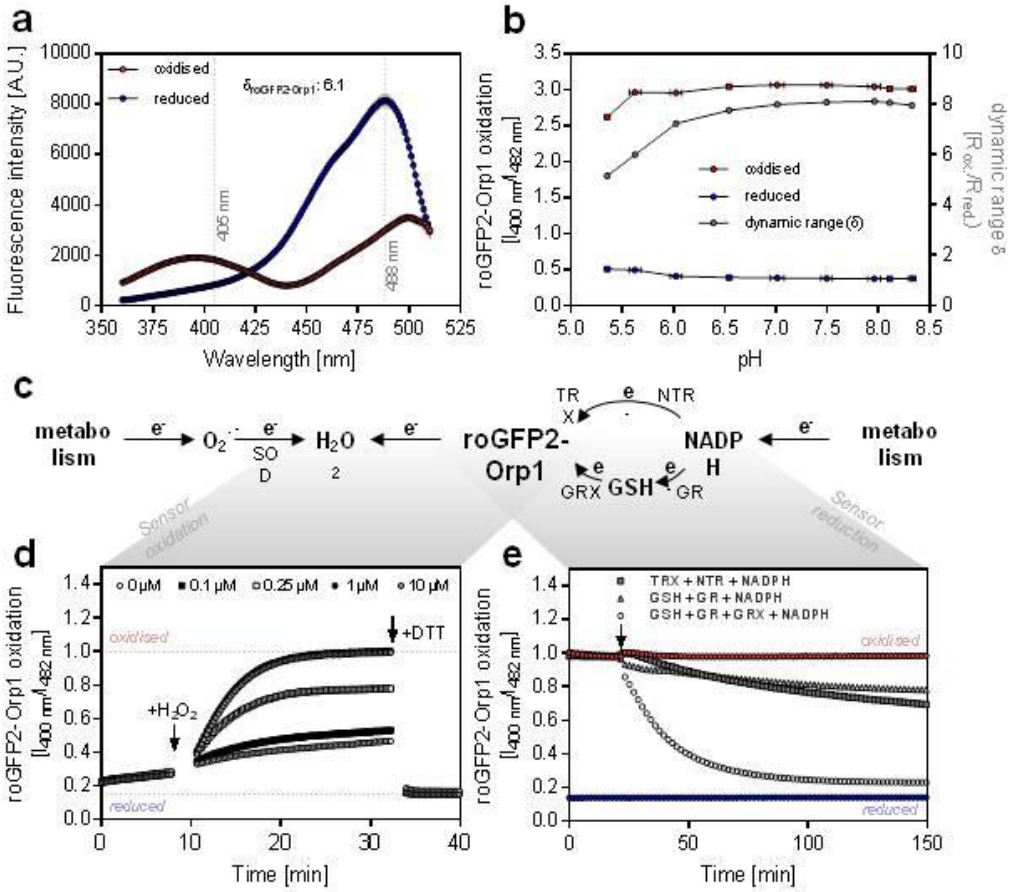

Figure 2

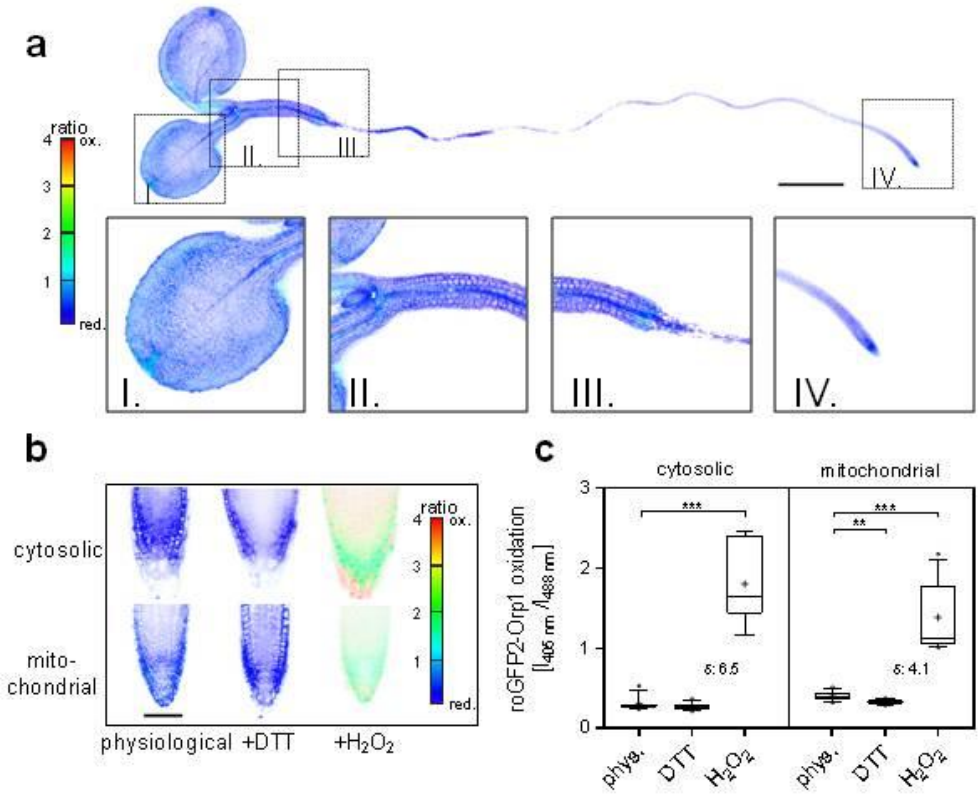

Figure 3

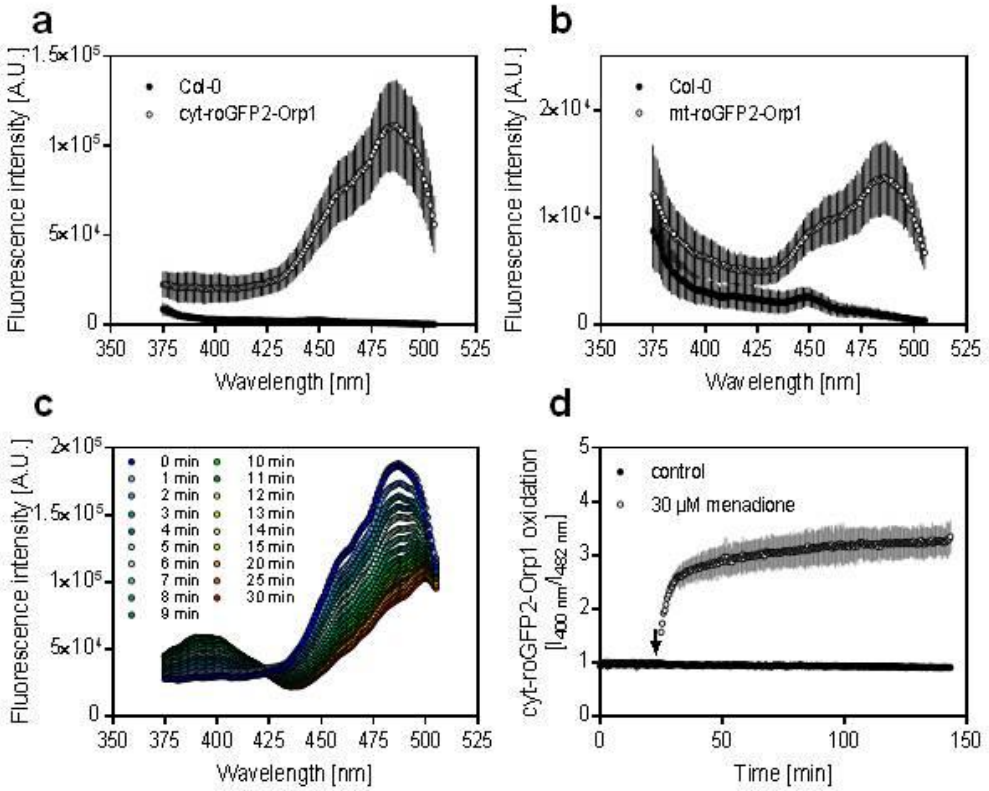

Figure 4

Figure 5

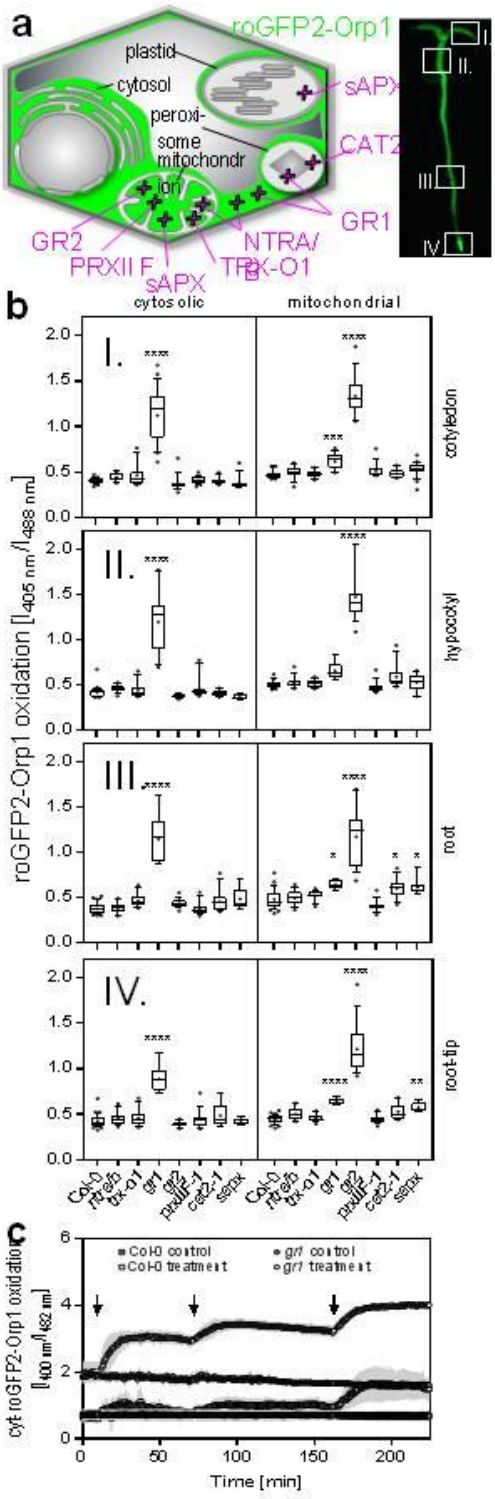

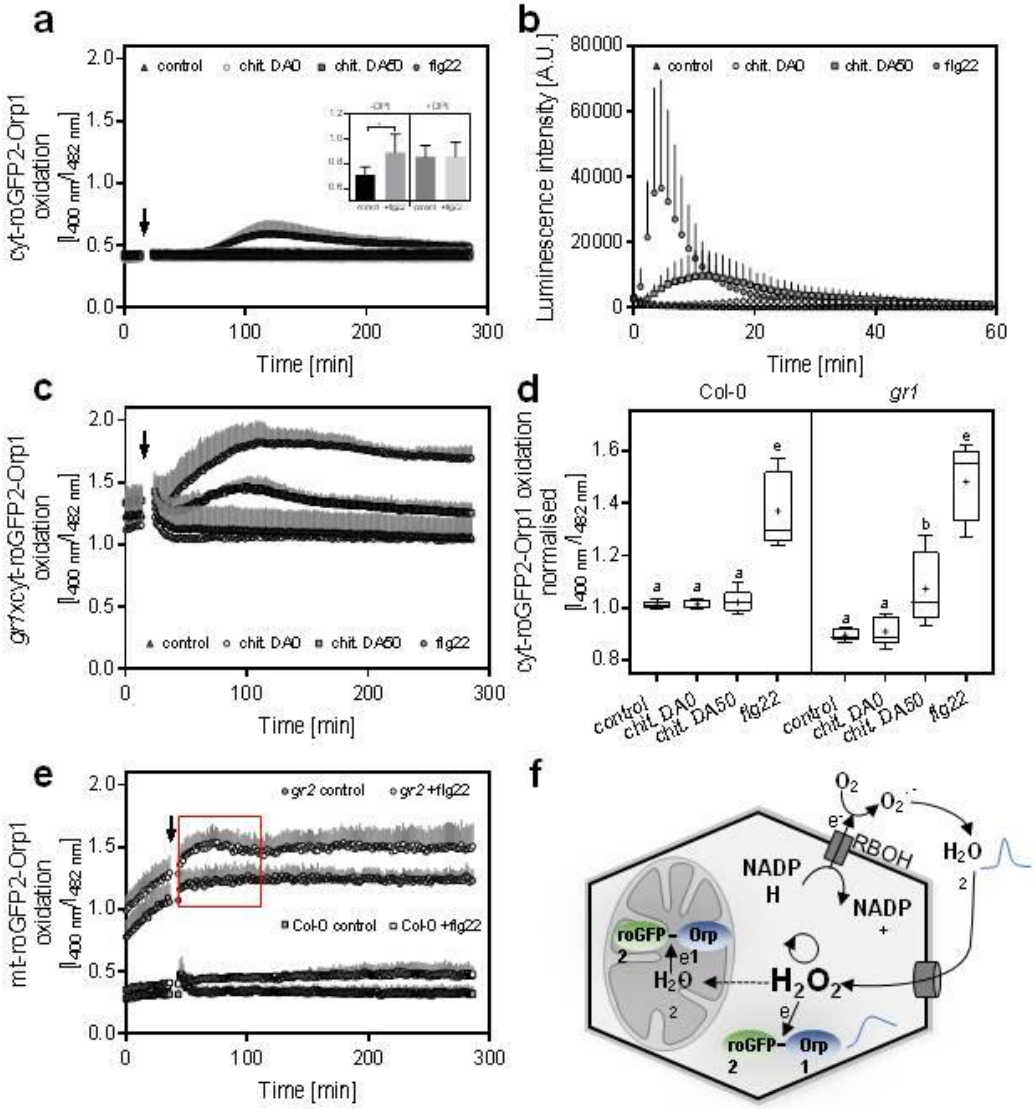

Figure 6